

② — — — — — 2

AD A050118



DEPARTMENT
OF
ELECTRICAL ENGINEERING

Ab No.
DDC FILE COPY

FINAL REPORT
A STUDY OF THE WAVEGUIDE MODE EXCITATION AND
PROPAGATION IN A PARALLEL PLATE TRANSMISSION LINE

PREPARED FOR
AIR FORCE OFFICE OF SCIENTIFIC RESEARCH
GRANT NUMBER AFOSR-76-3065

ENGINEERING AND
INDUSTRIAL RESEARCH STATION

DDC
FEB 17 1978
F

MISSISSIPPI STATE UNIVERSITY
STATE COLLEGE, MISSISSIPPI

Approved for public release;
distribution unlimited.

REPORT DOCUMENTATION PAGE		READ INSTRUCTIONS BEFORE COMPLETING FORM
1. REPORT NUMBER 18 AFOSR TR-78-0193 19	2. GOVT ACCESSION NO.	3. RECIPIENT'S CATALOG NUMBER
4. TITLE (and Subtitle) 6 A STUDY OF THE WAVEGUIDE MODE EXCITATION AND PROPAGATION IN A PARALLEL PLATE TRANSMISSION LINE	5. TYPE OF REPORT & PERIOD COVERED 9 Final rept.	
6. AUTHOR(s) 10 Terry T/Crow, Kuang Yuh Wu Claborne D/Taylor	7. PERFORMING ORG. REPORT NUMBER	
9. PERFORMING ORGANIZATION NAME AND ADDRESS Department of Electrical Engineering Mississippi State University Mississippi State, MS 39762	8. CONTRACT OR GRANT NUMBER(s) 15 AFOSR-76-3065	
11. CONTROLLING OFFICE NAME AND ADDRESS AFOSR/NP Bolling AFB, Bldg.#410 Wash DC 20332	10. PROGRAM ELEMENT, PROJECT, TASK AREA & WORK UNIT NUMBERS 9751-85 2301-93 61102F 16 17	
14. MONITORING AGENCY NAME & ADDRESS (if different from Controlling Office)	12. REPORT DATE 11 Nov 1977	
	13. NUMBER OF PAGES 61 1267p.	
	15. SECURITY CLASS (of this report) Unclassified	
15a. DECLASSIFICATION/DOWNGRADING SCHEDULE		
16. DISTRIBUTION STATEMENT (of this Report) Approved for public release; distribution unlimited.		
17. DISTRIBUTION STATEMENT (of the abstract entered in Block 20, if different from Report)		
18. SUPPLEMENTARY NOTES		
19. KEY WORDS (Continue on reverse side if necessary and identify by block number)		
20. ABSTRACT (Continue on reverse side if necessary and identify by block number) A study of the waveguide mode excitation and propagation is made for a parallel plate waveguide. Since this configuration is used in the simulation of the nuclear electromagnetic pulse, results appropriate for various simulators are obtained and discussed. The analysis assumes infinitely wide plates, but the question of finite width plates is addressed.		

A STUDY OF THE WAVEGUIDE MODE
EXCITATION AND PROPAGATION IN A
PARALLEL PLATE TRANSMISSION LINE

By

Terry T. Crow
Kuang Yuh Wu
Claborne D. Taylor



Prepared for
Air Force Office of Scientific Research
Bolling Air Force Base
Washington, D. C. 20332

November 1977

AIR FORCE OFFICE OF SCIENTIFIC RESEARCH (AFSC)
NOTICE OF TRANSMITTAL TO DDC
This technical report has been reviewed and is
approved for public release IAW AFR 190-12 (7b).
Distribution is unlimited.
A. D. BLOSE
Technical Information Officer

The research reported in this document was
sponsored under Grant number AFOSR-76-3065.

A STUDY OF THE WAVEGUIDE MODE
EXCITATION AND PROPAGATION IN A
PARALLEL PLATE TRANSMISSION LINE

ABSTRACT

A study of the waveguide mode excitation and propagation is made for a parallel plate waveguide. Since this configuration is used in the simulation of the nuclear electromagnetic pulse, results appropriate for various simulators are obtained and discussed. The analysis assumes infinitely wide plates, but the question of finite width plates is addressed.

ACCESSION for	
NTIS	Write Section <input checked="" type="checkbox"/>
DPC	Duff Section <input type="checkbox"/>
UNANNOUNCED	<input type="checkbox"/>
JUSTIFICATION	
DISTRIBUTION/AVAILABILITY CODES	
SOCIAL	
A	

TABLE OF CONTENTS

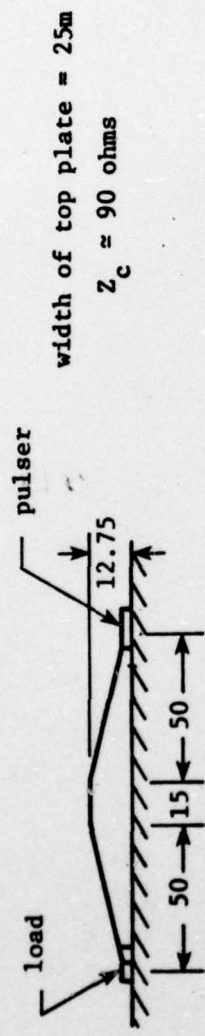
	Page
1. Introduction	2
2. Electromagnetic Fields in an Infinite, Parallel Plate Waveguide with a Single Conical Input Section	6
a. Physical Model	6
b. Mathematical Model	6
c. Frequency Domain	10
d. Time Domain, Magnetic Field	13
e. Time Domain, Electric Field	18
f. Comparison of Experimental Data and Theoretical Results for the ALECS Facility	37
3. Electromagnetic Fields in an Infinite, Parallel Plate Waveguide with a Double Conical Input Section	39
a. Physical Model	39
b. Mathematical Model	39
c. Time Domain, Magnetic Field	42
d. Time Domain, Electric Field	44
e. Numerical Results for the ATLAS I Simulator	44
References	59

1. Introduction

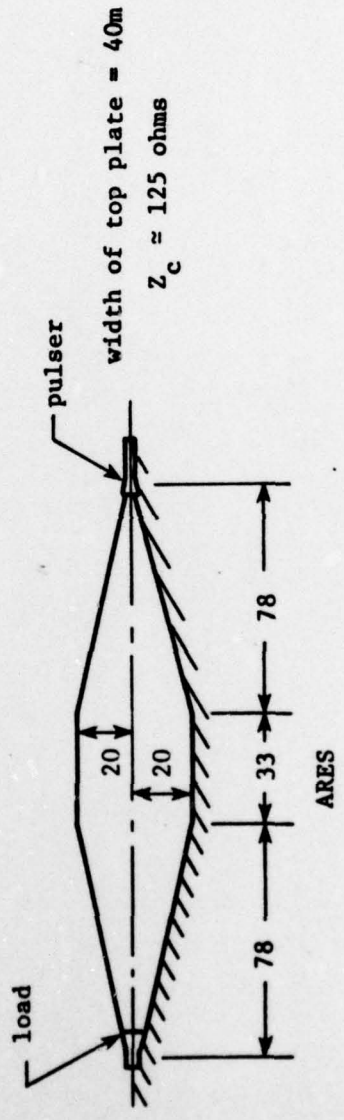
The parallel plate transmission line provides a useful means for measuring the electromagnetic field interaction. In this configuration nearly uniform electric and magnetic fields are produced, and instrumentation can be placed beneath one of the plates. There is, however, a practical problem associated with the design and excitation of the parallel plate transmission line; namely, one must provide a transition section, typically one or two conical transmission line sections, between the source and the parallel plate configuration (see Figures 1 and 2).

Insofar as the transmission line mode is concerned the transition section poses no problems provided the conical line and the parallel plates have approximately the same cross sectional shape at their interface and provided there is a match between the characteristic impedances. However, the spherical wavefront propagating along the conical line does not match the planar wavefront of the TEM mode in the parallel plate region, hence the excitation of TE and TM waveguide modes as well as the TEM mode occurs. Finally, in some situations a single input section is not sufficient to produce the required field strengths. In these cases (usually wide plate separations), dual input sections are used. When using dual input sections one must allow provision in the analysis for the fact that the sources may not fire simultaneously.

In studying the interaction of complex electrical systems with the electromagnetic pulse generated by a nuclear detonation, the parallel plate waveguide can be used to simulate the interaction. The electromagnetic pulse may be simulated by driving the parallel plates from

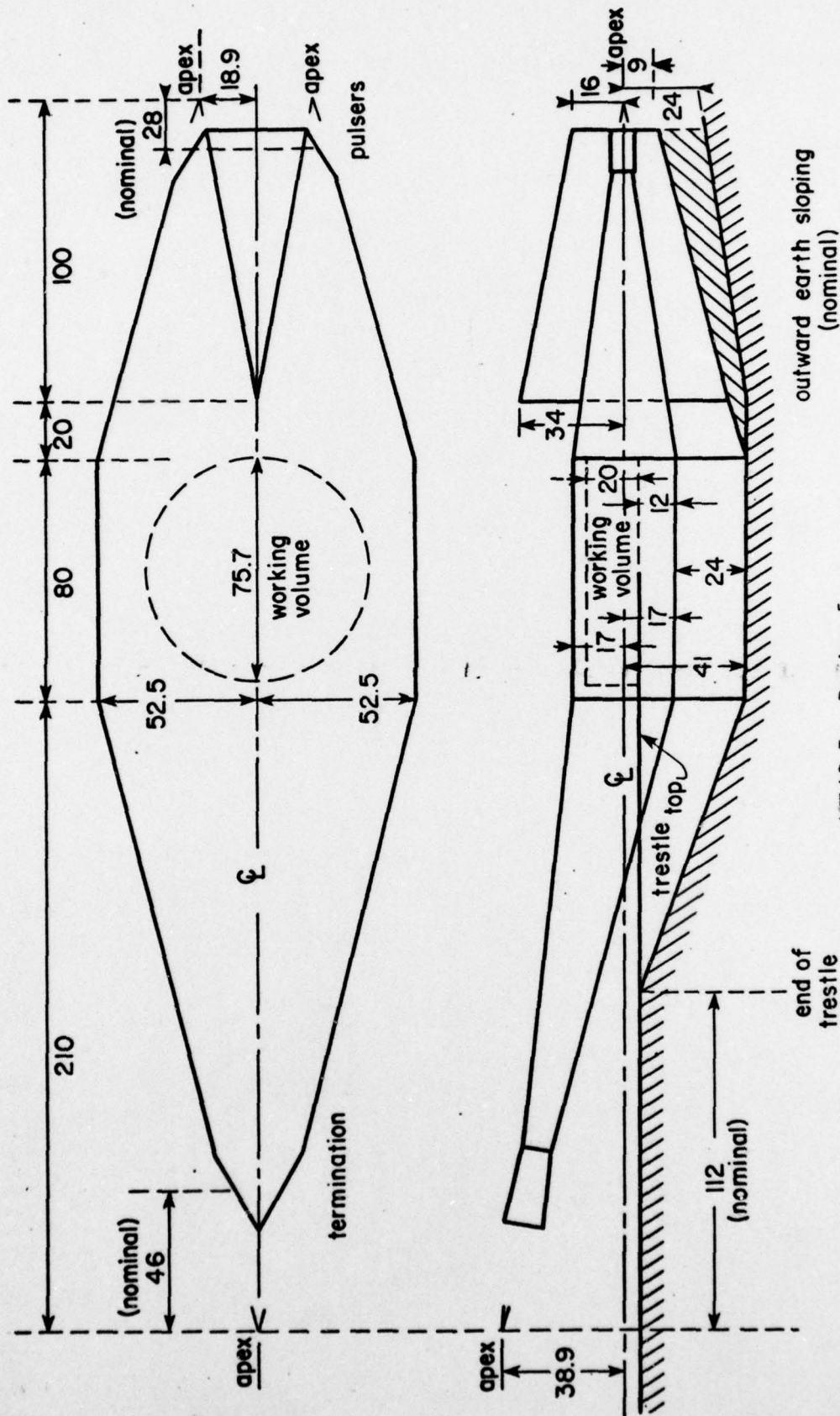


ALECS



ARES

Figure 1. Schematic Diagram of Two Parallel Plate Simulators. Note that all dimensions are in meters and the scale is 1cm = 25m.



ATLAS I: Design 5

Figure 2. Schematic Diagram of a Simulator with Dual Transitions Sections.
(All dimensions are in meters)

conical input sections with appropriate surge generators. There are a number of these simulation facilities currently in use. Example geometries for single and dual input parallel plate transmission line simulators are shown in Figures 1 and 2.

An additional complicating feature of these simulators is that they are constructed as finite width parallel plate transmission lines. The properties of the TEM mode on such a structure have been studied extensively [1,2]. Other studies [3] have shown that the waveguide modes for open region waveguides differ considerably from the modes of the more familiar closed region waveguides. The excitation coefficients for the modes in an open region structure are obtained by matching boundary conditions at the interface between the conical input section and the parallel plate region as well as on the waveguide walls [3]. Apparently, integral equations must be solved numerically to obtain the coefficients and propagation constants. Due to the complexity of these problems, the finite-width parallel plate configuration is approximated by using infinitely wide plates. However expected differences resulting in the data that are obtained are noted and discussed.

The analysis that is presented is validated by comparisons with measured data and with data obtained by other investigators.

2. Electromagnetic Fields in an Infinite, Parallel Plate

Waveguide with a Single Conical Input Section

a. Physical Model

One wishes to obtain the electric and magnetic fields in the parallel plate region of the structure shown in Figure 3 in terms of known quantities in the input section and the physical dimensions of the parallel plates.

Several simplifying assumptions are made. The plates are assumed to be perfectly conducting, the analysis is performed in the plane ASB of Figure 3, the wavefronts are assumed spherical in the conical section and written as

$$\bar{E}(x,z) = V_o \frac{e^{-jkr}}{r} \hat{\theta} \quad (1)$$

where $r^2 = x^2 + (z + z_o)^2$ (see Figure 4). Also, it is assumed there are no reflections in the conical section from the parallel plate region, and the electric field in the aperture AMB, Figure 4, is assumed to be a planar section of a spherical wavefront.

b. Mathematical Model

If one assumes the apex of the conical input pulser generates spherical waves, a magnetic current source \bar{M} - independent of y - is located at the plane $z = 0$ and \bar{M} is given by [4]

$$\bar{M} = \bar{E}_a \times \hat{n} \quad (2)$$

where \bar{E}_a is the electric field strength at the aperture or in the plane $z = 0$. From the method of images,

$$\bar{M} = 2 \bar{E}_a \times \hat{n} = -2(\bar{E}_a \cdot \hat{x}) \hat{y} = M_y \hat{y} \quad (3)$$

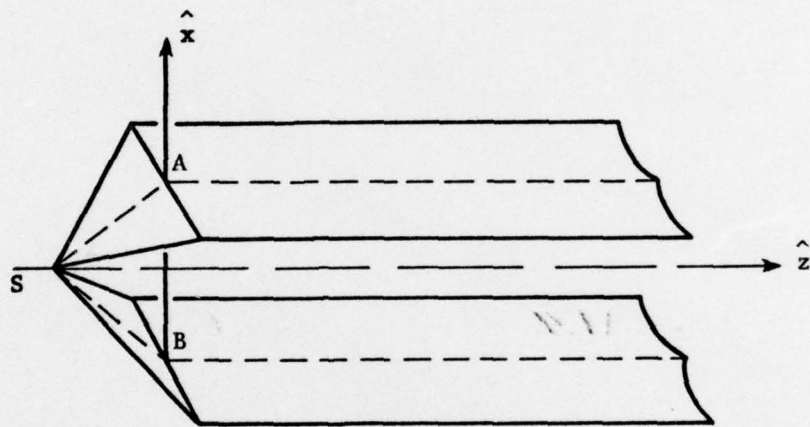


Figure 3. A Parallel-Plate Waveguide with a Single Conical Input Section.

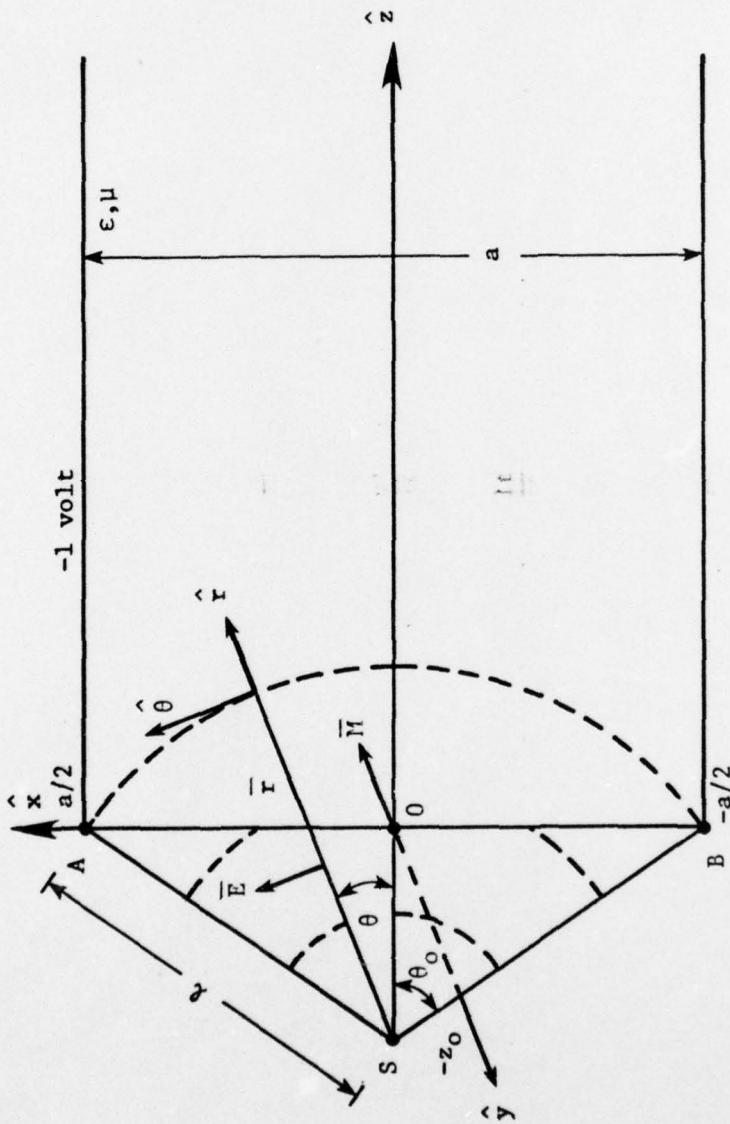


Figure 4. Two-Parallel-Plate Waveguide with a Single Pulser.
(Longitudinal section through apex S.)

Substitution of (1) into (3) yields

$$M_y = -2V_o \frac{e^{-jkr_o}}{r_o} \hat{\theta} \cdot \hat{x} \quad (4)$$

Since $\hat{\theta} \cdot \hat{x} = \cos \theta = z_o/r_o$, it follows that

$$M_y = -2z_o V_o \frac{e^{-jkr_o}}{r_o^2} \quad (5)$$

where $r_o^2 = x^2 + z_o^2$. The constant V_o is defined by normalizing the voltage between the plates to unity: i.e.

$$V_{BA} = - \int_B^A \bar{E}(x,z) \cdot \overline{ds} = -1 \text{ v} \quad (6)$$

Choosing the spherical wavefront through A and B as the path of integration, i.e., $r_o = \ell$, one finds

$$V_o = \frac{e^{jkl}}{2\theta_o} \quad (7)$$

and

$$M_y = \frac{-z_o}{\theta_o(x^2 + z_o^2)} e^{-jk(\sqrt{x^2 + z_o^2} - \ell)} \frac{v}{m} \quad (8)$$

For a charge and current free medium, Maxwell's equations are

$$\begin{aligned} \nabla \cdot \bar{D} &= 0 \\ \nabla \cdot \bar{B} &= 0 \\ \nabla \times \bar{E} &= -j\omega\mu \bar{H} - \bar{M} \\ \nabla \times \bar{H} &= j\omega\epsilon \bar{E} \end{aligned} \quad (9)$$

where ϵ and μ are the free space values of permittivity and permeability, and the time dependence $e^{j\omega t}$ is understood but suppressed. Since \bar{M} is y independent and the plates are assumed to be infinite in extent in the y direction, Maxwell's equations must be y independent. Thus, for TM waves

$$(\nabla_{xz}^2 + k^2) H_y = j\omega\epsilon M_y \quad (10)$$

$$E_x = -\frac{1}{j\omega\epsilon} \frac{\partial H_y}{\partial z} \quad (11)$$

$$E_z = \frac{1}{j\omega\epsilon} \frac{\partial H_y}{\partial x} \quad (12)$$

where $\nabla_{xz}^2 = \frac{\partial^2}{\partial x^2} + \frac{\partial^2}{\partial z^2}$ and $k = 2\pi/\lambda = \omega/c$.

c. Frequency Domain

The standard technique for solving (10) is the Green's function method; i.e., H_y is replaced by $G(x, z|x', 0)$ and M_y is replaced by $\delta(x-x')\delta(z)$. Thus, to find G , one must solve

$$(\nabla_{xz}^2 + k^2) G(x, z|x', 0) = j\omega\epsilon \delta(x-x')\delta(z) \quad (13)$$

Additionally, G must satisfy the same boundary conditions as H_y , or

$$(i) \quad \frac{\partial G}{\partial x} = 0 \quad @ \quad x = \pm a/z$$

$$(ii) \quad \int_{-\infty}^{\infty} |G|^2 dz < \infty$$

G is assumed to be a Fourier series of even and odd terms

$$G = \sum_{n=0,2,4,\dots} \left(\frac{\epsilon_n}{a}\right)^{\frac{1}{2}} b_n^e(z) \cos \frac{n\pi x}{a} + \sum_{n=1,3,5,\dots} \left(\frac{2}{a}\right)^{\frac{1}{2}} b_n^o(z) \sin \frac{n\pi x}{a} \quad (14)$$

with superscripts e and o representing even and odd integers respectively, and

$$\begin{aligned} \epsilon_n &= 1 & \text{if } n &= 0 \\ &= 2 & \text{if } n &\neq 0 \end{aligned}$$

The solution of (13) for the even terms in G is

$$G^e(x, z | x', 0) = -\frac{\omega \epsilon}{a} \sum_{n=0,2,4,\dots} \frac{\epsilon_n}{2} \cos \frac{n\pi x'}{a} \cos \frac{n\pi x}{a} \frac{e^{-jk_n z}}{R_n} \quad (15)$$

where $k_n^2 = k^2 - (n\pi/a)^2$. To obtain H_y^e , one evaluates the integral

$$H_y^e(x, z) = \int_{-a/2}^{a/2} M_y(x') G^e(x, z | x', 0) dx' \quad (16)$$

It follows that

$$H_y^e(x, z) = \frac{z \omega \epsilon e^{jk\ell}}{\theta_o a} \sum_{n=0,2,4,\dots} \left(\frac{\epsilon_n}{2}\right) A_n^e \cos \frac{n\pi x}{a} \frac{e^{-jk_n z}}{k_n} \quad (17)$$

where

$$A_n^e = \int_{-a/2}^{a/2} \cos \frac{n\pi x'}{a} \frac{e^{-jk\sqrt{x'^2 + z_o^2}}}{x'^2 + z_o^2} dx' \quad (18)$$

Similarly, one can solve for the odd terms with the result

$$H_y^o(x, z) = \frac{z_o \omega \epsilon e^{jkl}}{\theta_o a} \sum_{n=1,3,5,\dots} A_n^o \sin \frac{n\pi x}{a} \frac{e^{-jk_n z}}{k_n} \quad (19)$$

and

$$A_n^o = \int_{-a/2}^{a/2} \sin \frac{n\pi x'}{a} \frac{e^{-jk\sqrt{x'^2 + z_o^2}}}{x'^2 + z_o^2} dx' \quad (20)$$

A_n^o for single cone excitation is identically zero; thus

$$H_y(x, z) = \frac{z_o \omega \epsilon e^{jkl}}{\theta_o a} \sum_{n=0,1,2,3,\dots} \epsilon_n A_n \cos \frac{2n\pi x}{a} \frac{e^{-jk_n z}}{k_n} \quad (21)$$

In (21) it should be observed that the summation is now over all integers, and

$$A_n = \int_0^{a/2} \cos \frac{2n\pi x'}{a} \frac{e^{-jk\sqrt{x'^2 + z_o^2}}}{x'^2 + z_o^2} dx' \quad (22)$$

and

$$k_n^2 = k^2 - (2n\pi/a)^2 \quad (23)$$

Use of (11) and (12) in conjunction with (21) leads to

$$E_x(x, z) = \frac{z_o e^{jkl}}{\theta_o a} \sum_{n=0}^{\infty} \epsilon_n A_n \cos \frac{2n\pi x}{a} e^{-jk_n z} \quad (24)$$

$$E_z(x, z) = \frac{2\pi j z_o e^{jkl}}{\theta_o a^2} \sum_{n=0}^{\infty} n A_n \sin \frac{2n\pi x}{a} \frac{e^{-jk_n z}}{k_n} \quad (25)$$

The first terms in (21), (24), and (25) represent the TEM mode and all remaining terms are TM modes. For finite-width parallel plates TE modes also are excited and propagated [3]. Moreover the TE modes are considerably less attenuated than the TM modes. For both sets, the modes are attenuated above cut-off due to the radiation from the open sides of the waveguide. Thus the results that are obtained for the infinitely wide plates must be interpreted carefully.

d. Time Domain, Magnetic Field

Having obtained the frequency domain results of section c, one can proceed in several ways to evaluate the time domain results. From (21) [and also (25) though this will not be discussed] one can solve the time domain problem analytically. From (24), one can evaluate the field at various frequencies and by means of numerical inverse Fourier transform [5] determine the behavior in the time domain.

Showing the ω -dependence explicitly, one can rewrite (21) as

$$H_y(x, z, \omega) = \frac{z_0}{\theta_0 a \eta} A_0(\omega) e^{j(\ell-z)\omega/c} + \sum_{n=1}^{\infty} j \frac{2z_0 \epsilon}{a \theta_0} \cos \frac{2n\pi x}{a} A_n(\omega) \omega F_n(z, \omega) \quad (26)$$

with

$$A_n(\omega) = \int_0^{a/2} \cos \frac{2n\pi x'}{a} \frac{e^{-j \frac{\omega}{c} \sqrt{x'^2 + z_0^2}}}{x'^2 + z_0^2} dx' \quad (27)$$

and

$$F_n(z, \omega) = \frac{e^{j\omega\ell/c} e^{-jz \sqrt{\frac{\omega^2}{c^2} - \left(\frac{2n\pi}{a}\right)^2}}}{j \sqrt{\frac{\omega^2}{c^2} - \left(\frac{2n\pi}{a}\right)^2}} \quad (28)$$

The expression in (26) is the frequency response at a particular ω or the response to a $\delta(t)$ input. The Fourier transform of the step function, $u(t)$

$$u(t) = \begin{cases} 0 & t < 0 \\ 1 & t \geq 0 \end{cases}$$

is

$$F[u(t)] = \frac{1}{a\pi} \left[\pi \delta(\omega) + \frac{1}{j\omega} \right] \quad (29)$$

from which it follows that the response to the step function excitation is

$$\begin{aligned} h_y^s(x, z, t) &= \frac{1}{2\pi} \int_{-\infty}^{\infty} \left[\pi \delta(\omega) + \frac{1}{j\omega} \right] H_y(s, z, \omega) e^{j\omega t} d\omega \\ &= h_y^{so} + \sum_{n=1}^{\infty} h_y^{sn} \end{aligned} \quad (30)$$

where o and n refer to the zeroth or n th term. Rewriting the h_y^{so} and collecting terms in a convenient manner, one obtains

$$h_y^{so} = \frac{z_o}{\theta_o a \eta} \int_0^{a/2} \frac{1}{x'^2 + z_o^2} \left\{ \frac{1}{2\pi} \int_{-\infty}^{\infty} \left[\pi \delta(\omega) + \frac{1}{j\omega} \right] e^{j\omega f(t, \ell, z, x')} d\omega \right\} dx' \quad (31)$$

and

$$f(t, \ell, z, x') = t + (\ell - z)/c - \sqrt{x'^2 + z_o^2}/c$$

Thus, (31) becomes

$$h_y^{so} = \frac{z_o}{\theta_o a \eta} \int_0^{a/2} \frac{1}{x'^2 + z_o^2} u \left(t + \frac{\ell - z}{c} - \frac{\sqrt{x'^2 + z_o^2}}{c} \right) dx' \quad (32)$$

and, since $l \geq \sqrt{x'^2 + z_0^2}$, then if $t \geq z/c$

$$h_y^{so} = \frac{1}{a\eta} \quad t \geq z/c \quad (33)$$

In general one must evaluate (32) subject to the condition that

$$ct \geq \sqrt{x'^2 + z_0^2} + z - l$$

Since x' varies, this means the integral must be done in one of three ways depending on the time, t .

1. If $ct < z_0 + z - l$, the integral in (32) is identically zero.
2. If $z_0 + z - l < ct < \sqrt{\left(\frac{a}{2}\right)^2 + z_0^2} + z - l$, the upper limit on this integral is

$$x_u = \sqrt{(ct + l - z)^2 - z_0^2}.$$

3. If $ct \geq \sqrt{\left(\frac{a}{2}\right)^2 + z_0^2} + z - l$, the upper limit on the integral is $a/2$.

These statements are basically causality conditions.

Using the identity $\delta(\omega) \phi(\omega) = \delta(\omega) \phi(0)$, one finds

$$h_y^{sn} = \int_0^{a/c} \frac{\cos \frac{2n\pi x'}{a}}{x'^2 + z_0^2} dx' \cdot \frac{c}{2\pi j} \cdot \int_{-\infty}^{\infty} \frac{e^{-jz\sqrt{\frac{\omega^2}{c^2} - \left(\frac{2n\pi}{a}\right)^2}} e^{j\omega[ct + l - \sqrt{x'^2 + z_0^2}]} d\left(\frac{\omega}{c}\right)}{\sqrt{\frac{\omega^2}{c^2} - \left(\frac{2n\pi}{a}\right)^2}} \quad (34)$$

The second integral in (34) can be transformed analytically [6] using the identity

$$\frac{1}{2\pi j} \int_{-\infty}^{\infty} \frac{e^{-jx\sqrt{\omega^2 - y^2}}}{\sqrt{\omega^2 - y^2}} e^{j\omega t} d\omega = J_0(y\sqrt{t^2 - x^2}), \quad t > x \quad (35)$$

The final result of these manipulations is

$$h_y^s(x, z, t) = \frac{1}{a\eta} f_1 + \frac{2z_0}{\theta_0 a\eta} \sum_{n=1}^{\infty} \cos \frac{2n\pi x}{a} \int_0^{x'} \cos \frac{2n\pi x'}{a} \frac{1}{x'^2 + z_0^2} \cdot J_0 \left\{ \frac{2n\pi}{a} \sqrt{(ct + \ell - \sqrt{x'^2 + z_0^2})^2 - z^2} \right\} dx' \quad (36)$$

Again, the integral in (36) must be evaluated subject to the same conditions discussed for (32), and f_1 depends on the evaluation of (32) (e.g., if $ct \geq \sqrt{\left(\frac{a}{2}\right)^2 + z_0^2} + z - \ell$, then $f_1 = 1$). The expression for h_y^s , (36), must be evaluated numerically. First, define a new function $\Psi(N)$ which is identical to h_y^s except the summation runs from one to N rather than from one to infinity. The function $\Psi(N)$ versus N is shown in Figure 5. The function calculated in the program is defined as

$$h_y^s(x, z, t) = \frac{\sum_{N=20}^{40} \Psi(N)}{21} \quad (37)$$

One other comment is appropriate. The integrals in (37) are evaluated using a 15-point Gauss-Legendre quadrature formula. As n increases, the function to be evaluated oscillates more rapidly. Therefore, a change of variable is performed such that as n increases, the number of Gauss-Legendre zones from $x' = 0$ to $x' = a/2$ increases proportional to n .

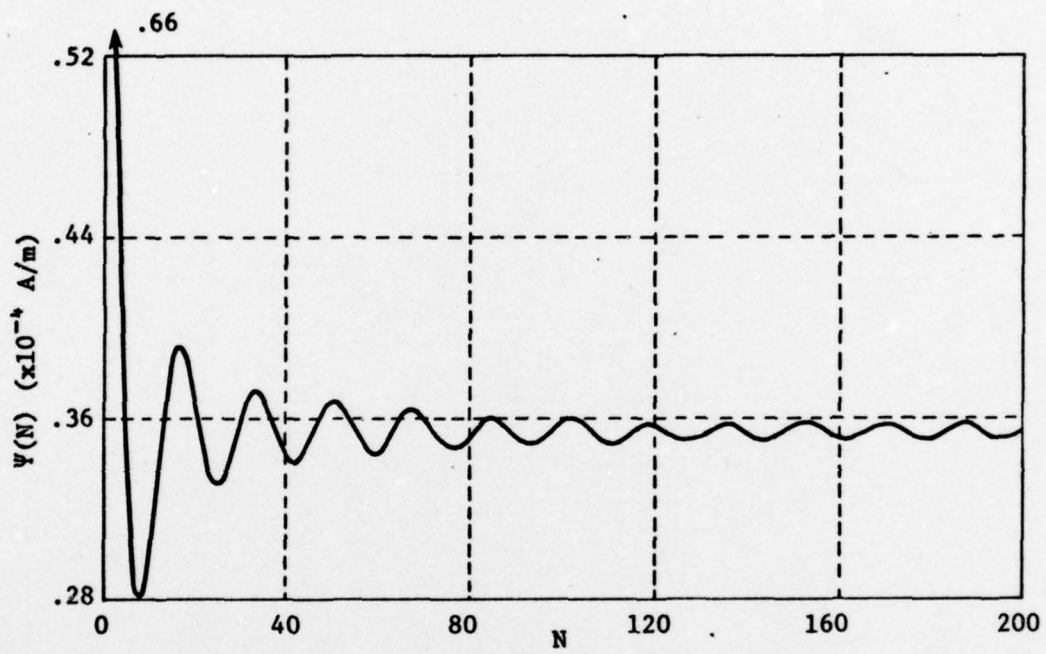


Figure 5. Plots of $\Psi(N)$ versus N . (with $a = 40$ m, $z_0 = 20$ m at $x = 0$ and $z = 50$ m for $t = 160$ ns)

The y component of the magnetic field, $h_y^s(x,z,t)$, due to a step function excitation is plotted with respect to time (t) and shown in Figures 6 for several field points in an ALECS-type facility, while Figure 7 is appropriate for the ARES geometry. Note that time is measured from $t = 0$, the time at which all the dipoles in the plane $z = 0$ have turned on. Corresponding frequency domain (Fourier Transforms of h_y) are shown in Figures 8 and 9. Note that singularities occur at the cavity resonances of the parallel plates.

e. Time Domain, Electric Field

The electric field calculations in the time domain have been performed using the inverse Fourier transform rather than an analytic solution. $E_x(x,z,\omega)$, (24), has been evaluated for 100 different frequencies varying from the d-e term to 100 MHz. The frequencies chosen were as follows:

f	Δf
0	-
.5 - 1 MHz	.1 MHz
1 - 10 MHz	.2 MHz
10 - 100 MHz	2 MHz

$e_x(x,z,t)$ has been evaluated using standard Fourier transform techniques: in this procedure it is assumed that $E_x(x,z,\omega)$ is a linear function of frequency between the individual calculated field values [5]. Since $E_x(x,z,\omega)$ as given by (24) is the impulse response then it must be multiplied by the Fourier transform of the actual pulse driving the plates--in the previous section this pulse was assumed to be a unit step.

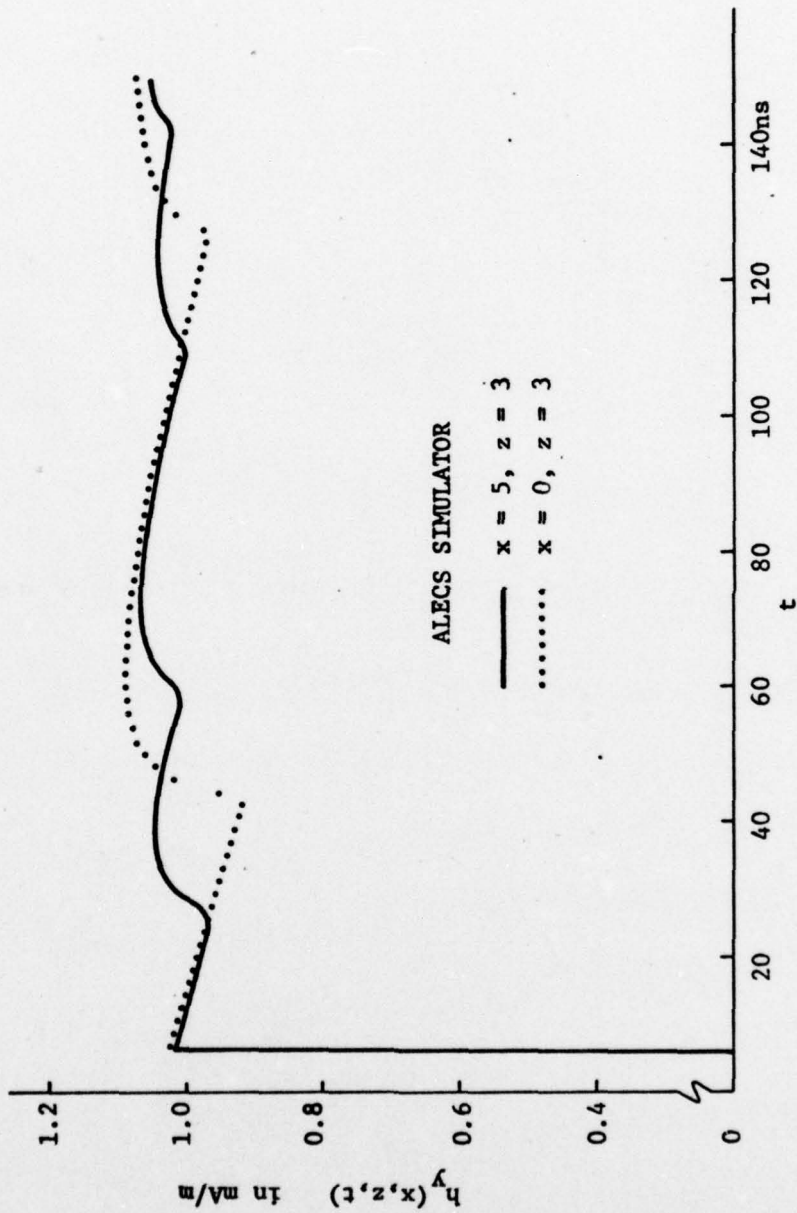


Figure 6: The horizontal magnetic field produced by a unit step excitation of the ALECS simulator.

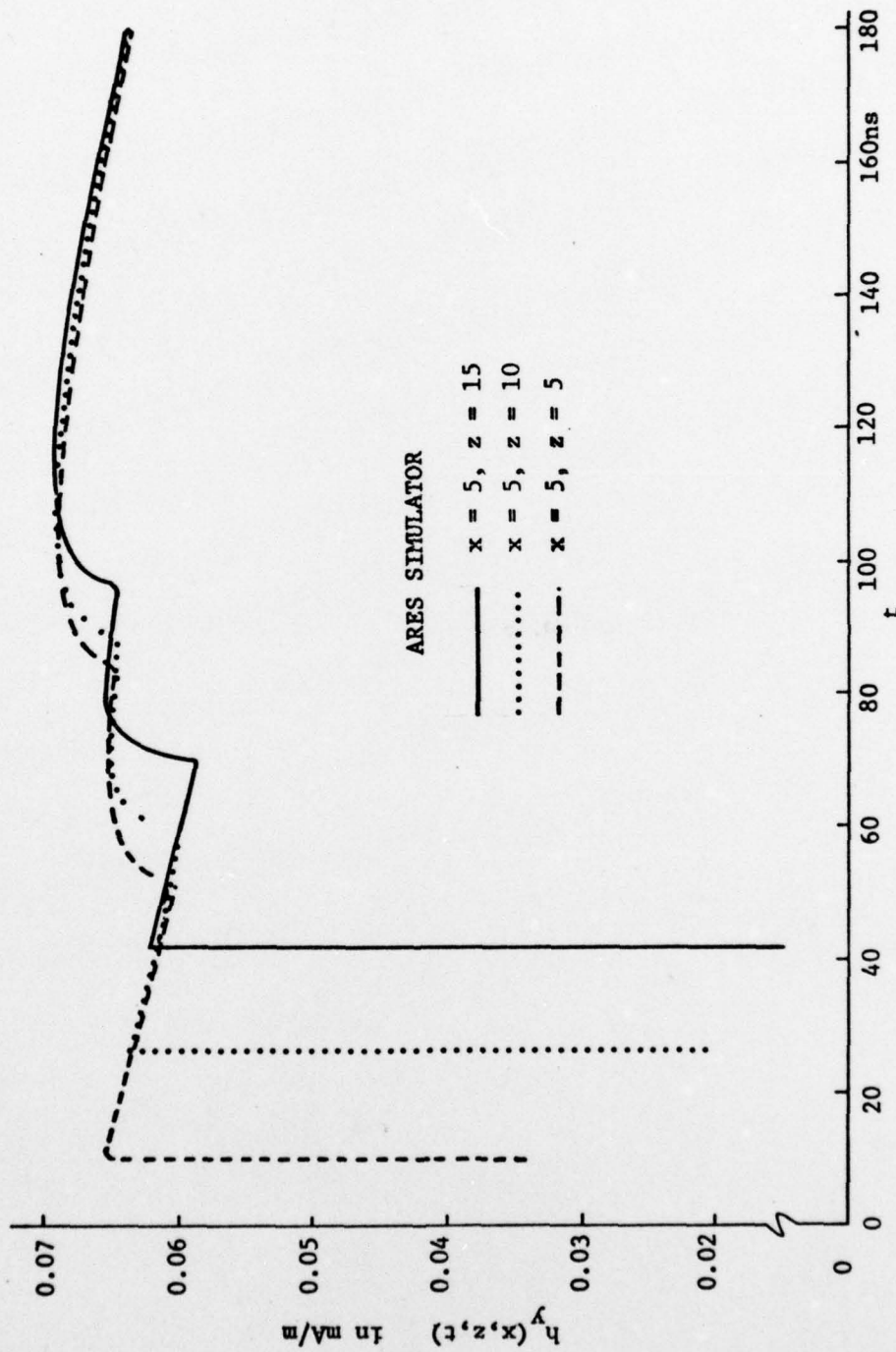


Figure 7: The horizontal magnetic field produced by a unit step excitation of the ARES simulator.

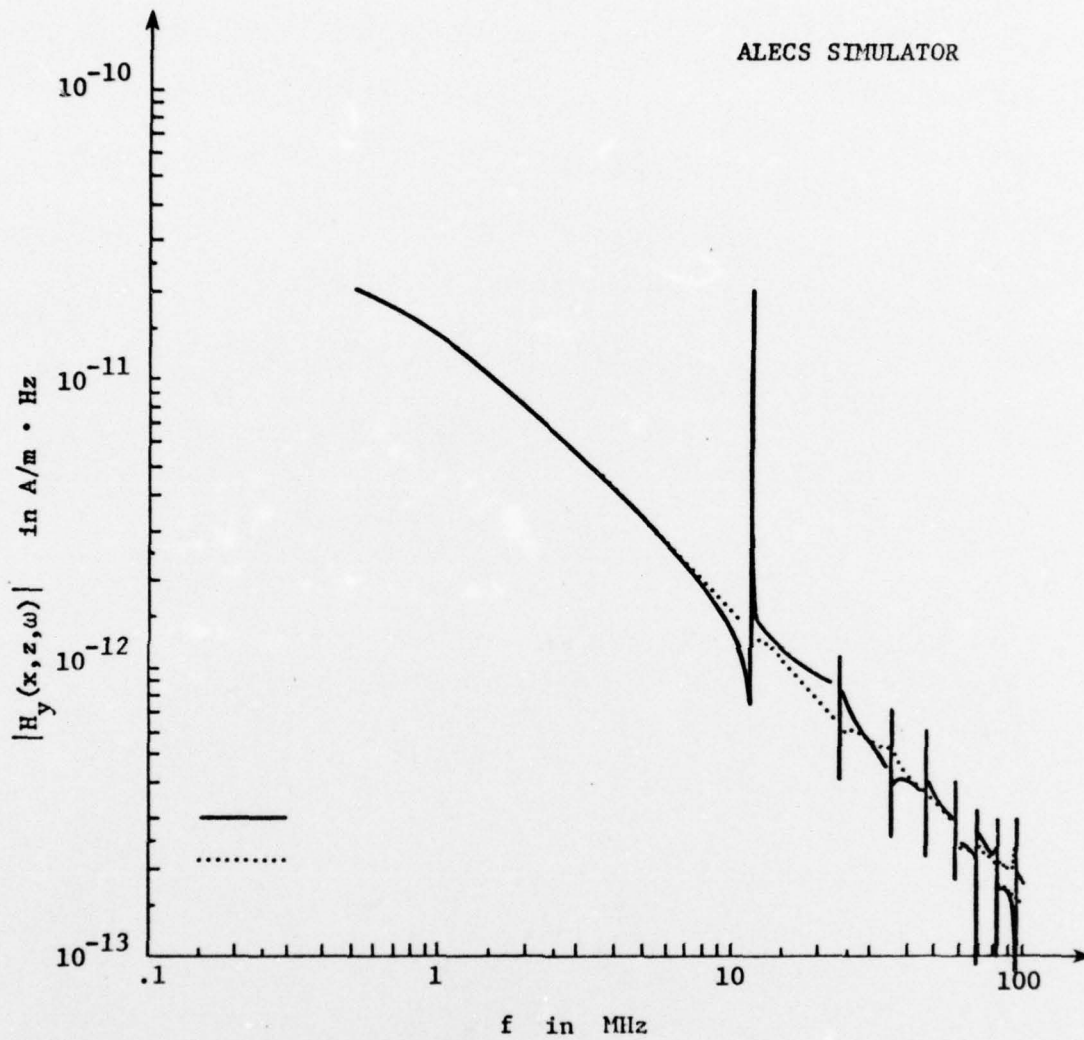


Figure 8: The Fourier transform of the horizontal magnetic field produced by a unit step excitation of the ALECS simulator.

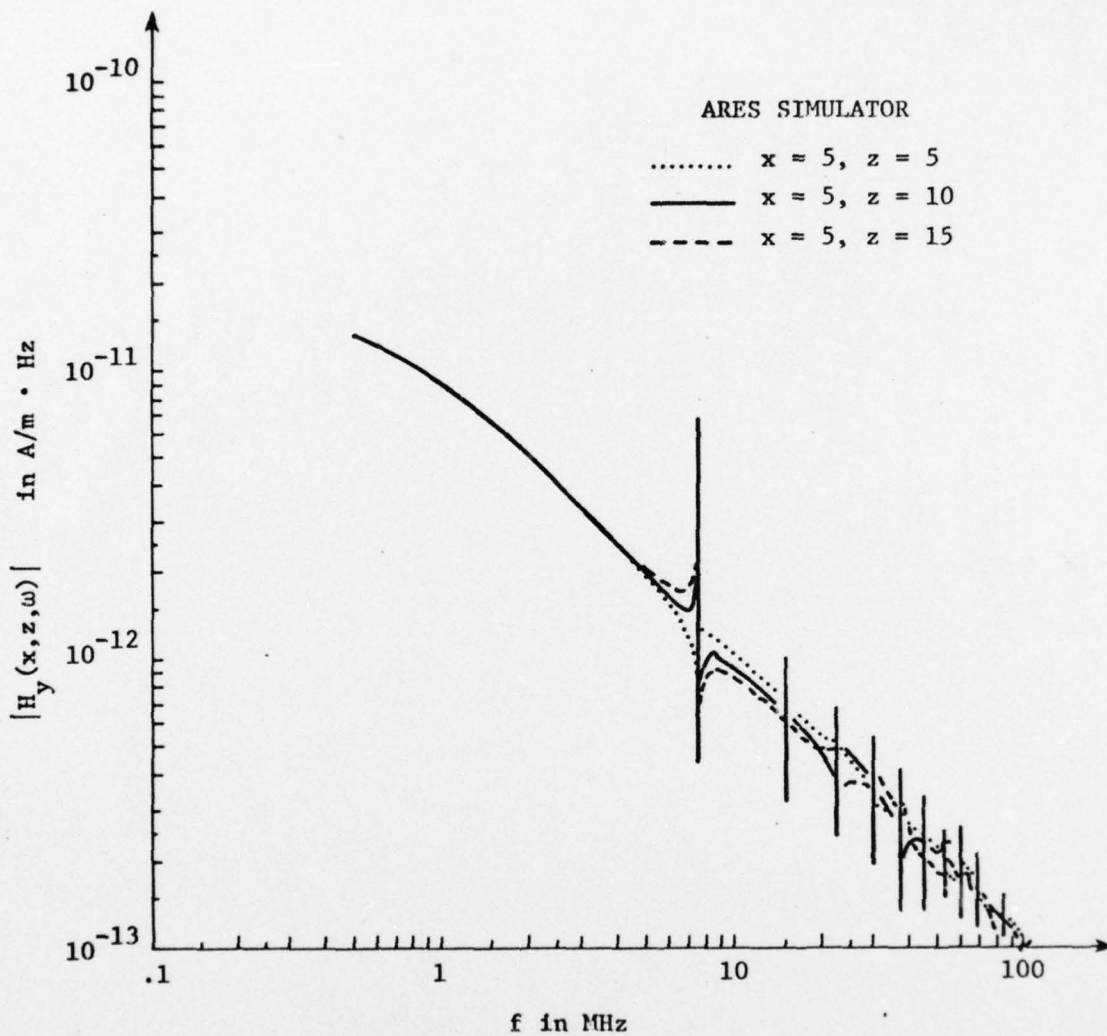


Figure 9: The Fourier transform of the horizontal magnetic field produced by a unit step excitation of the ARES simulator.

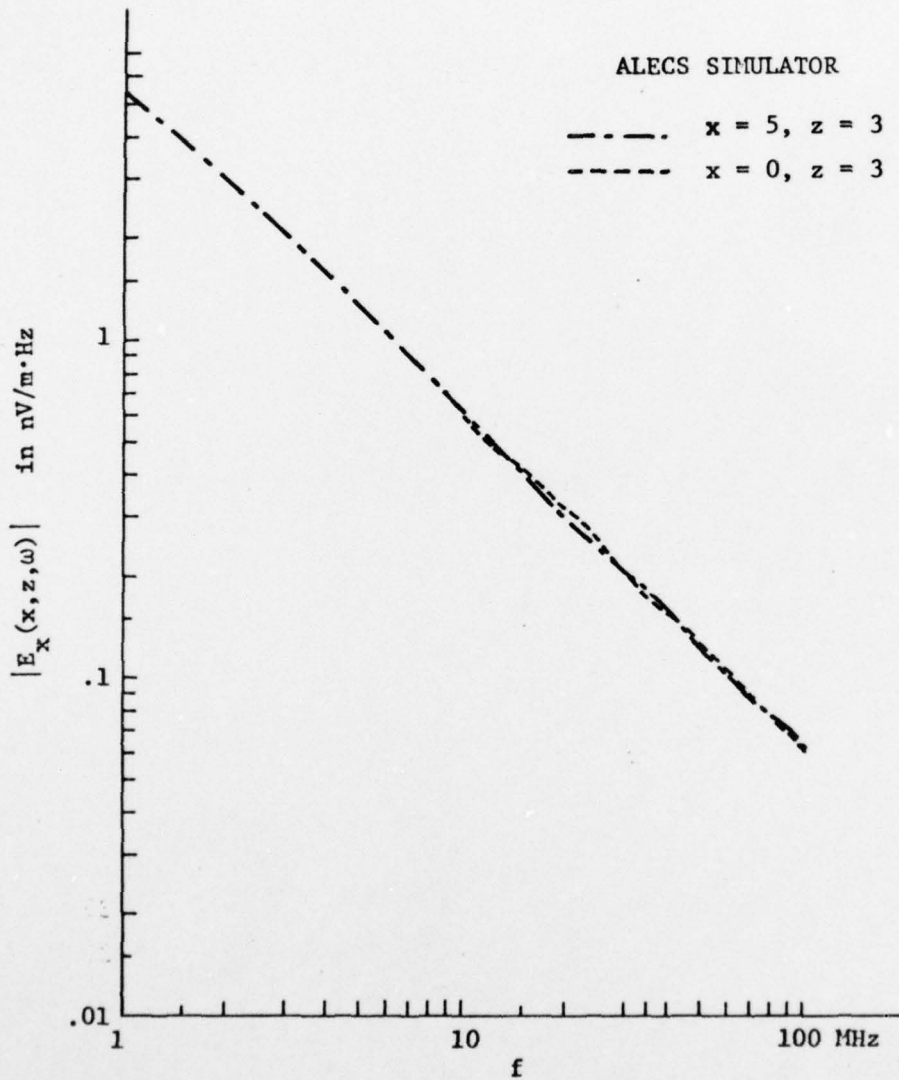


Figure 10: The Fourier transform of the vertical electric field produced by a unit step (with exponential decay) excitation of the ALECS simulator.

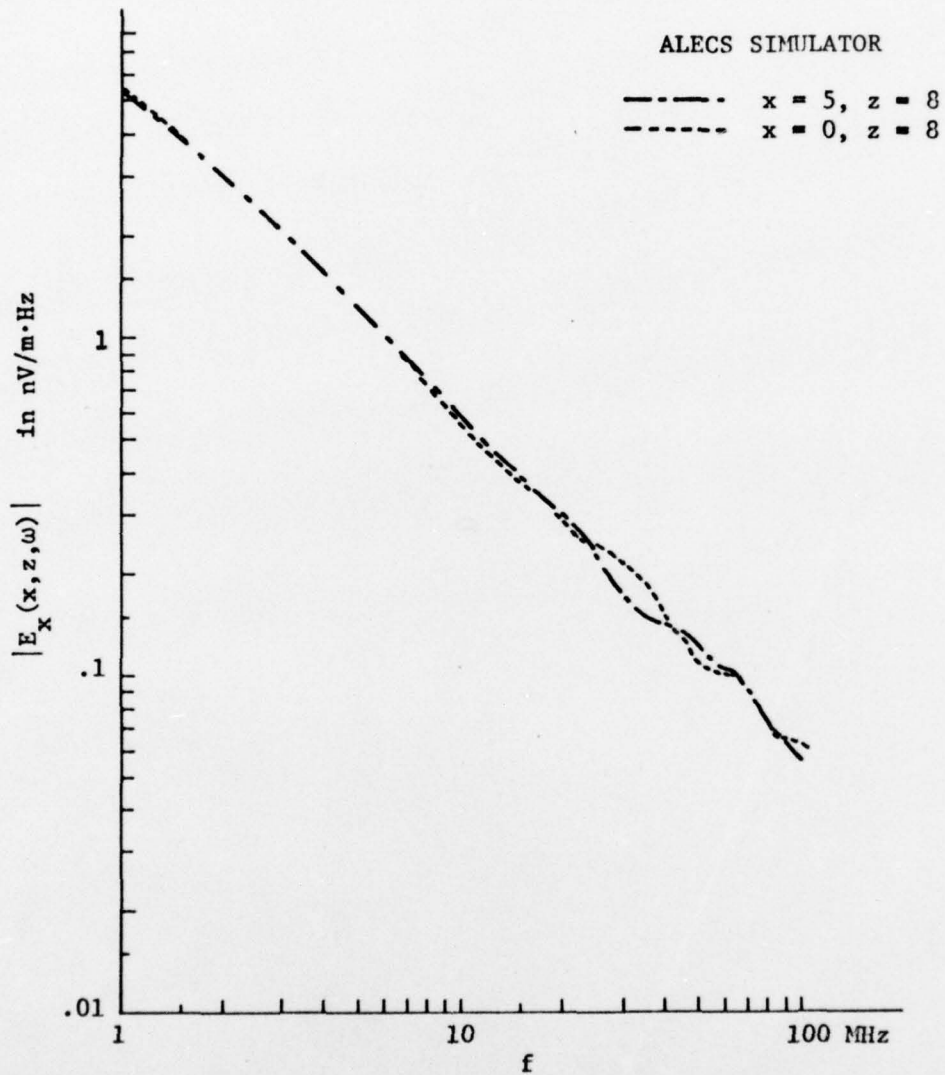


Figure 11: The Fourier transform of the vertical electric field produced by a unit step (with exponential decay) excitation of the ALECS simulator.

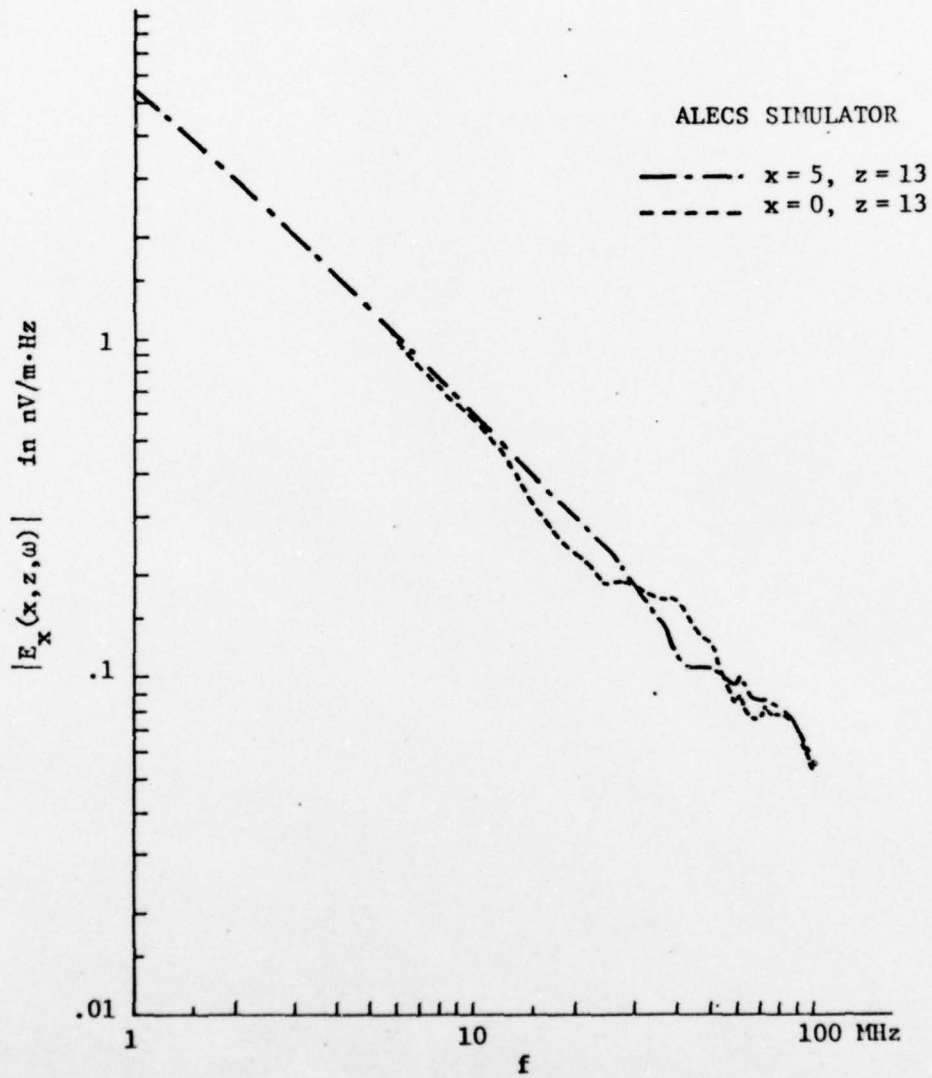


Figure 12: The Fourier transform of the vertical electric field produced by a unit step (with exponential decay) excitation of the ALECS simulator.

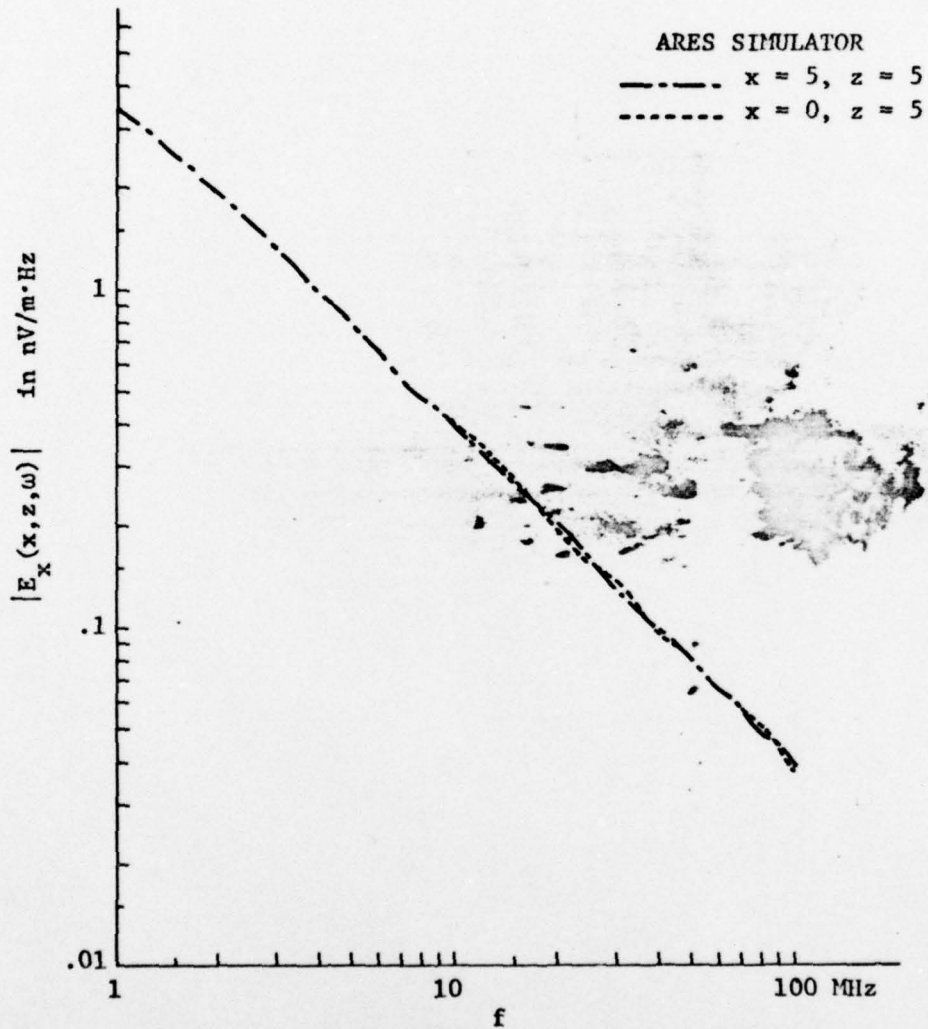


Figure 13: The Fourier transform of the vertical electric field produced by a unit step (with exponential decay) excitation of the ARES simulator.

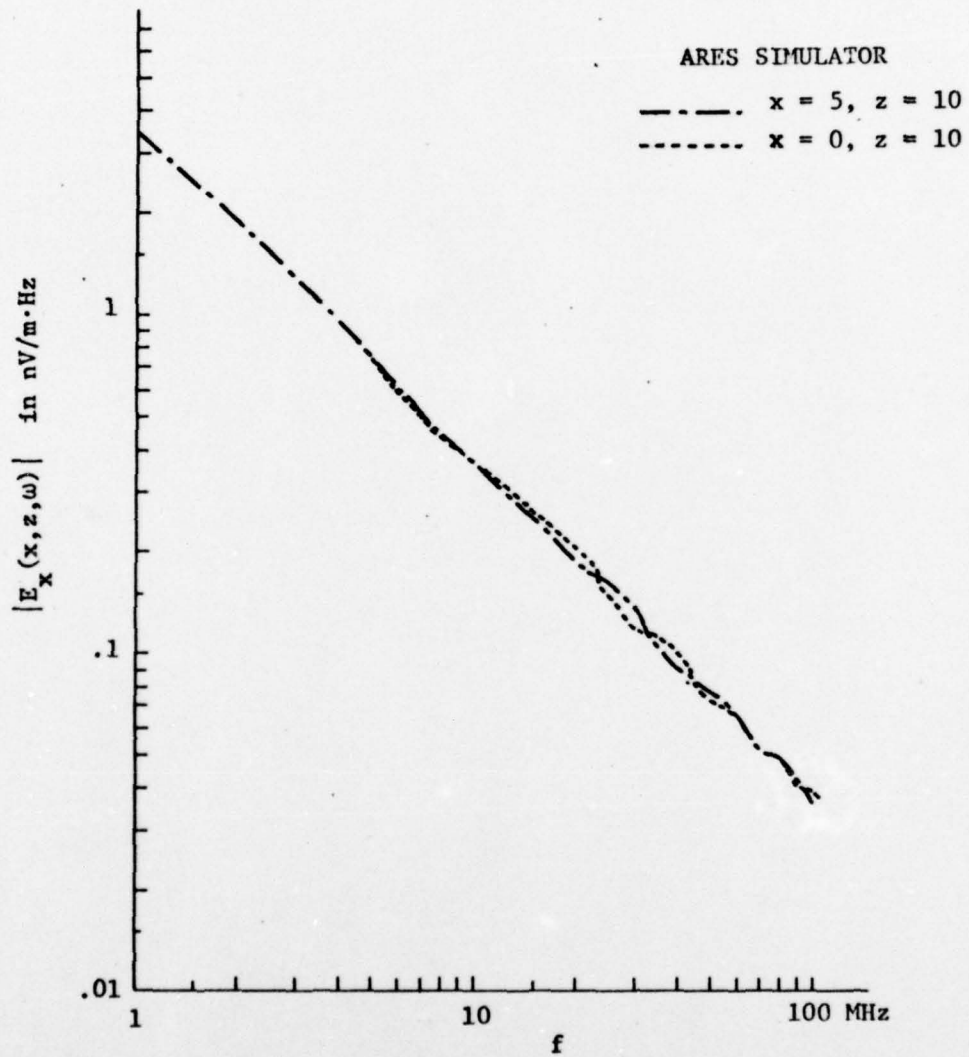


Figure 14: The Fourier transform of the vertical electric field produced by a unit step (with exponential decay) excitation of the ARES simulator.

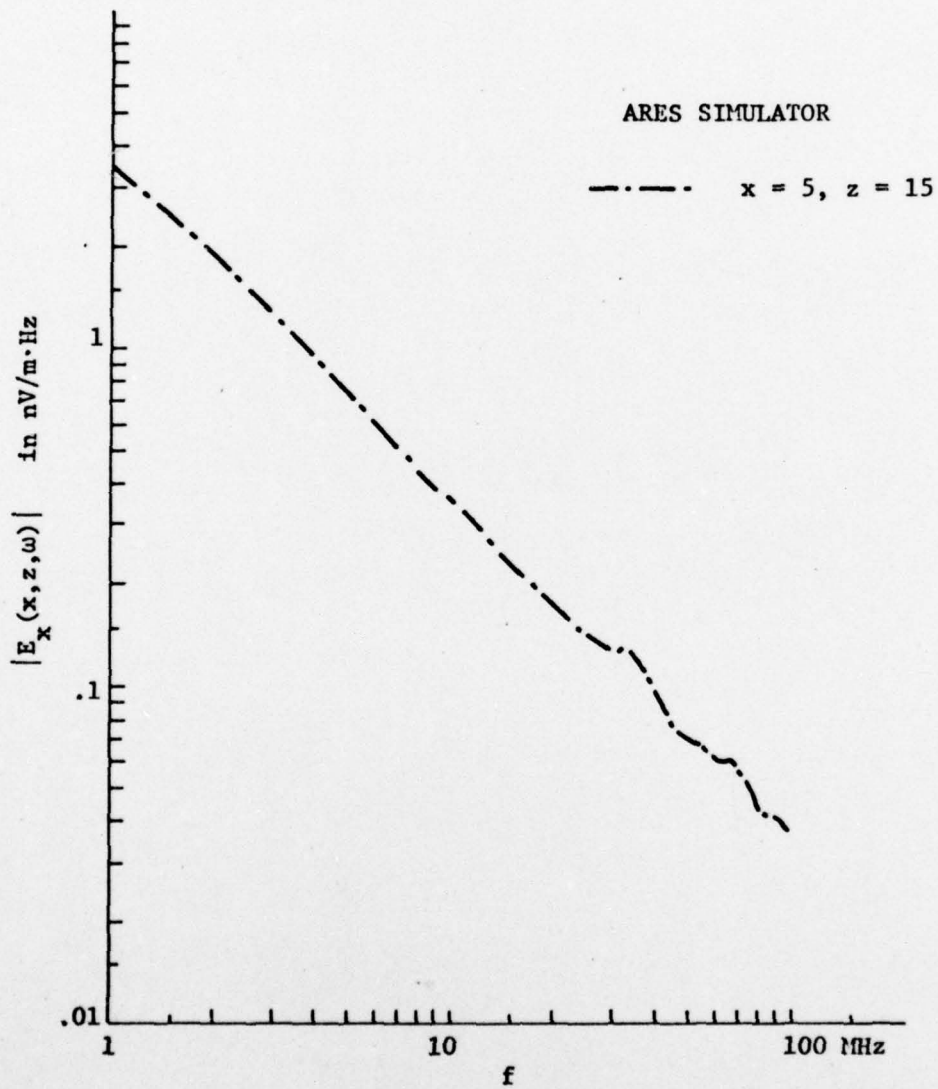


Figure 15: The Fourier transform of the vertical electric field produced by a unit step (with exponential decay) excitation of the ARES simulator.

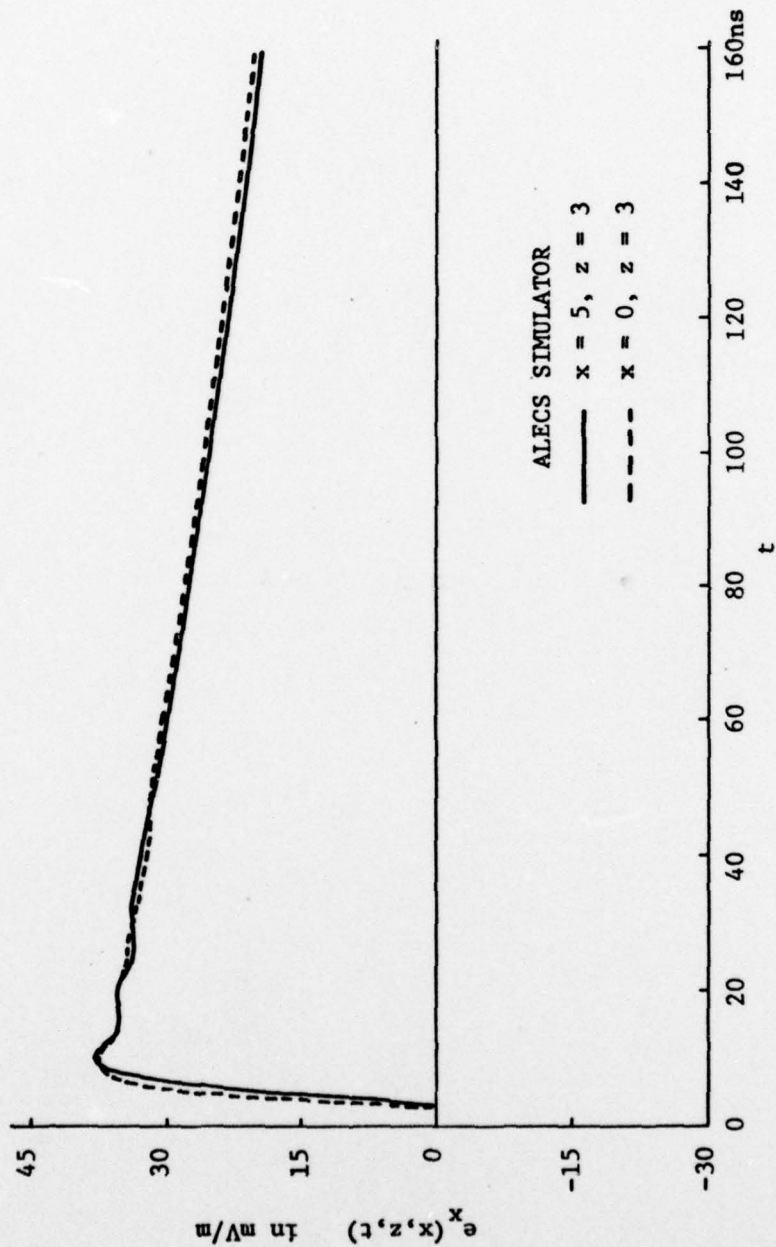


Figure 16: The vertical electric field produced by a unit step (with exponential decay) excitation of the ALECS simulator.

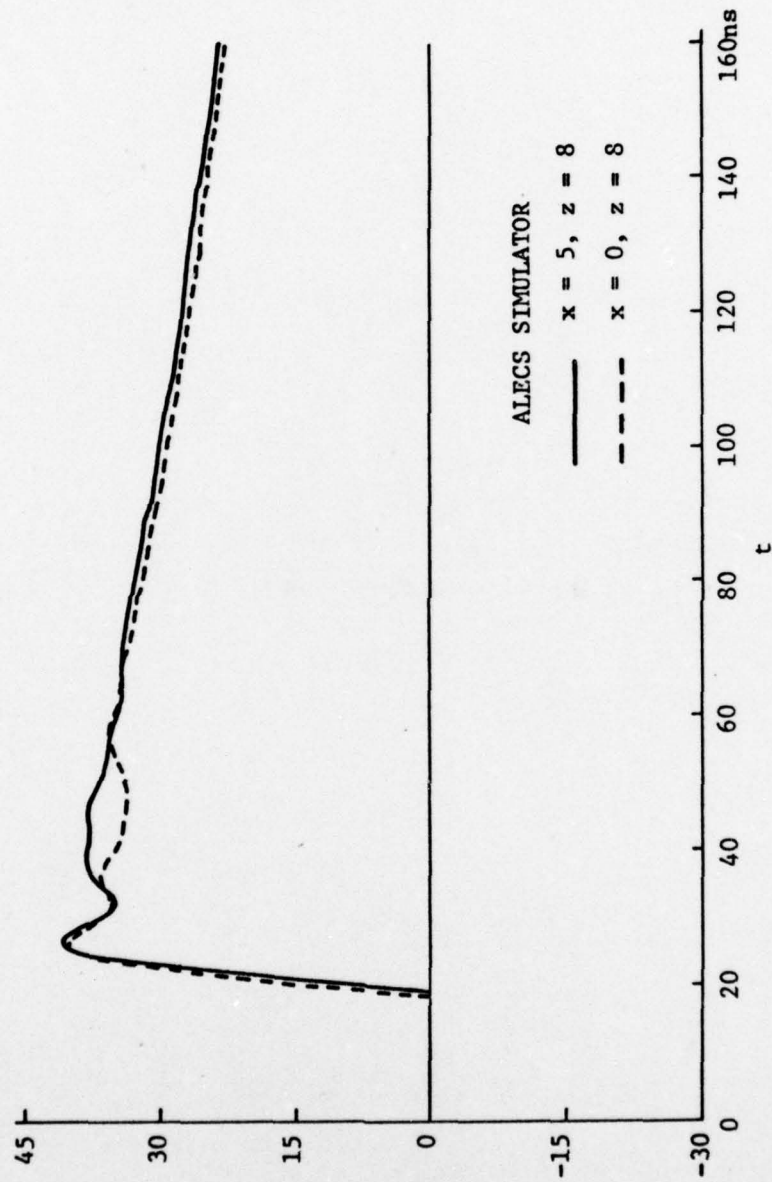


Figure 17: The vertical electric field produced by a unit step (with exponential decay) excitation of the ALECS simulator.

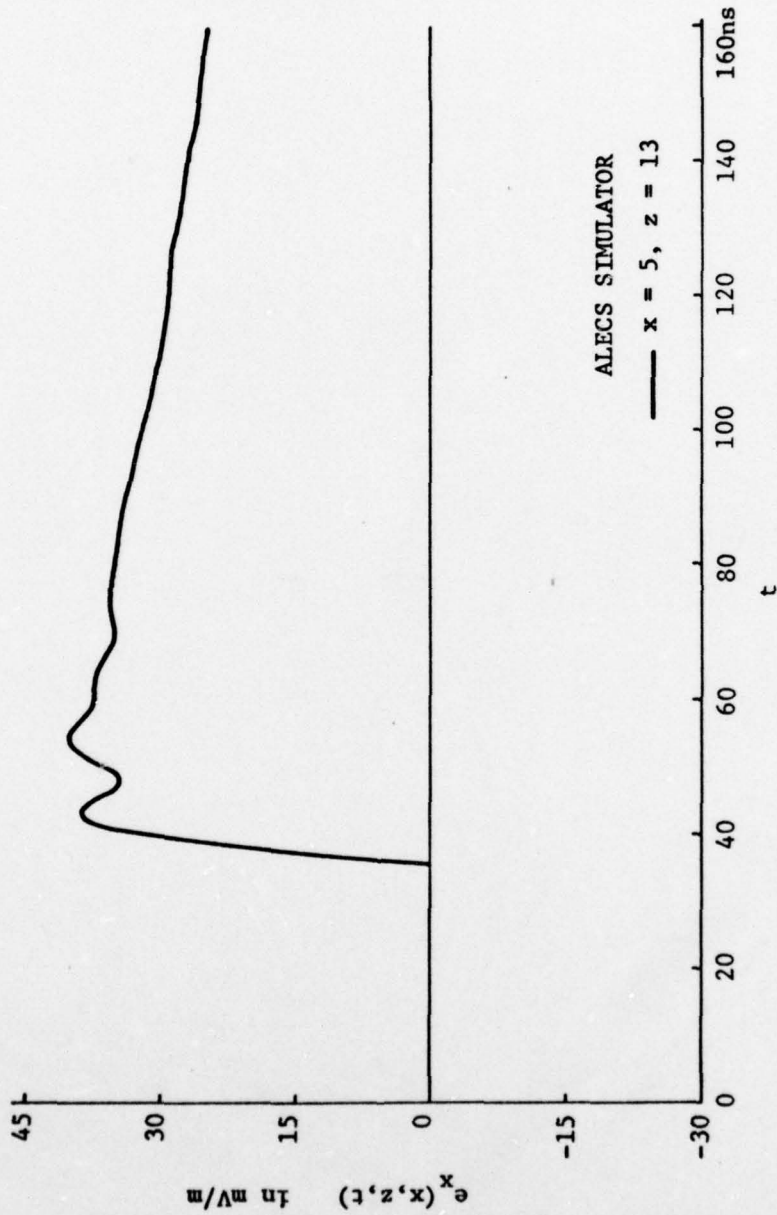


Figure 18: The vertical electric field produced by a unit step (with exponential decay) excitation of the ALECS simulator.

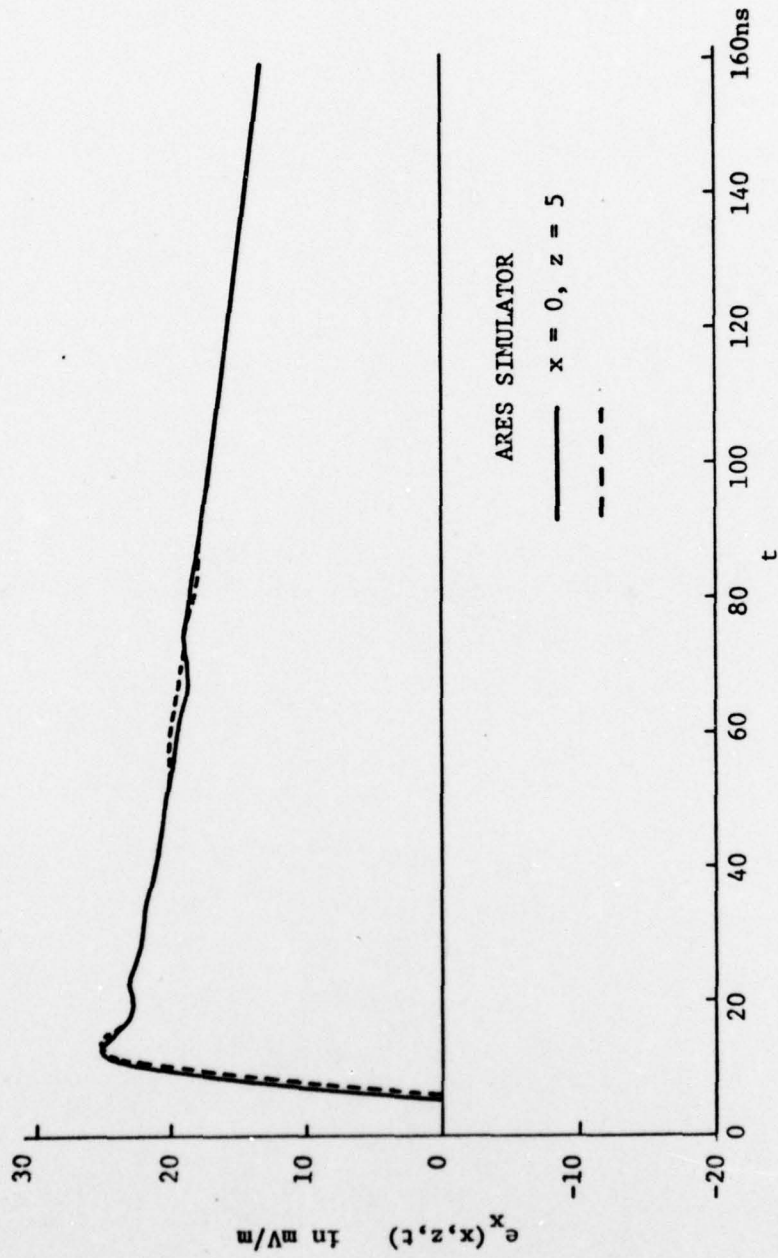


Figure 19: The vertical electric field produced by a unit step (with exponential decay) excitation of the ARES simulator.

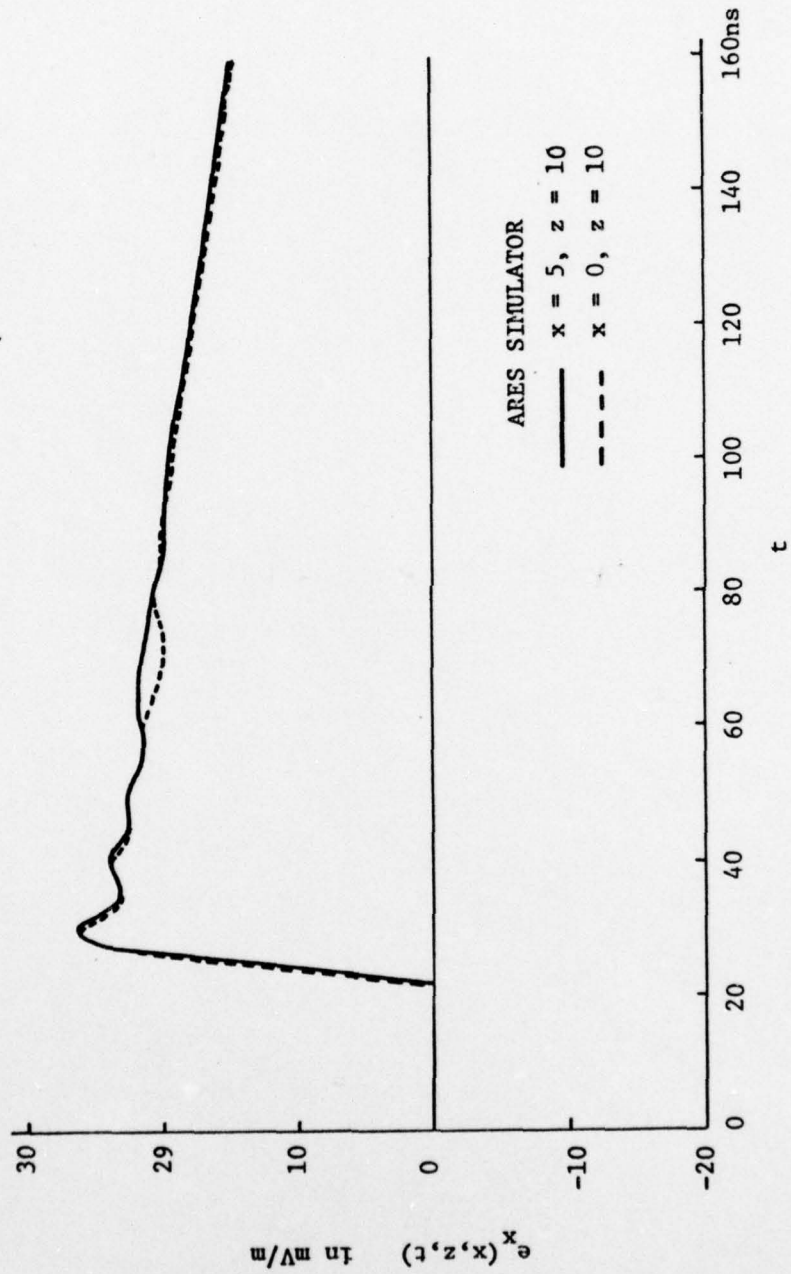


Figure 20: The vertical electric field produced by a unit step (with exponential decay) excitation of the ARES simulator.

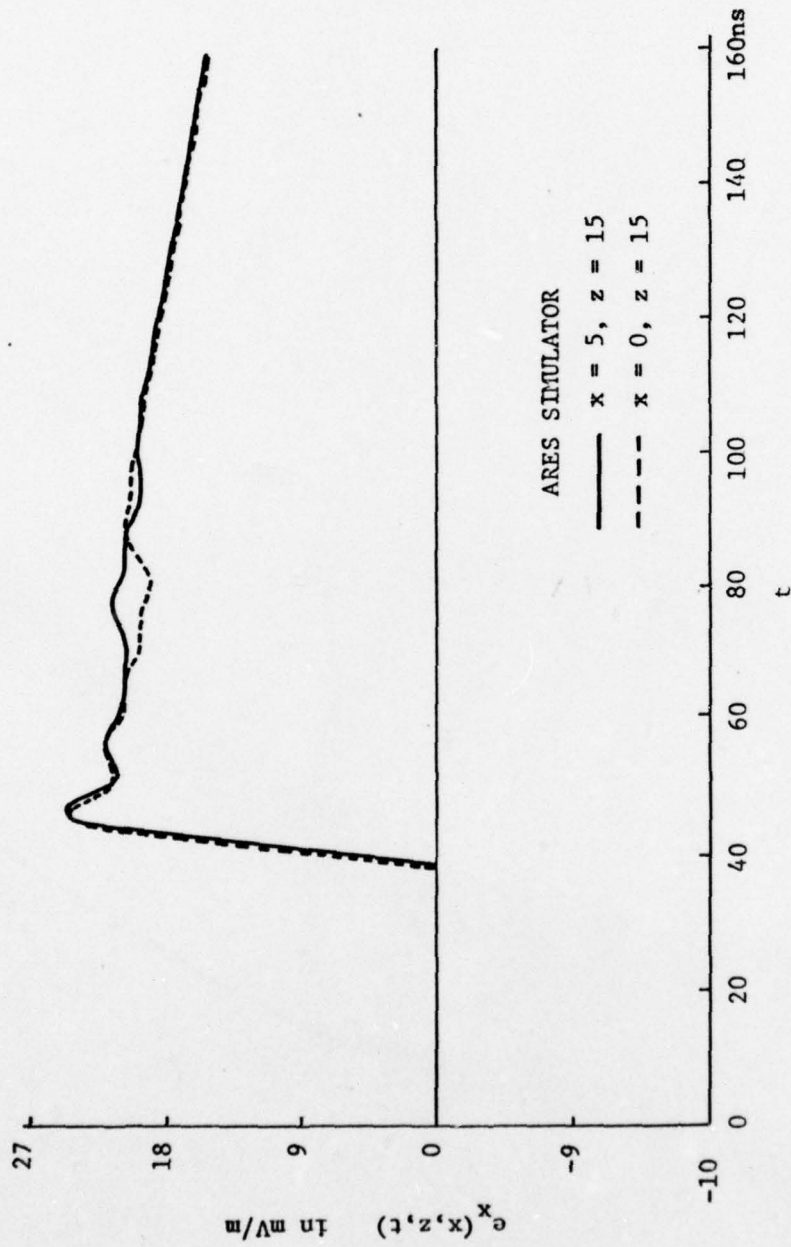


Figure 21: The vertical electric field produced by a unit step (with exponential decay) excitation of the ARES simulator.

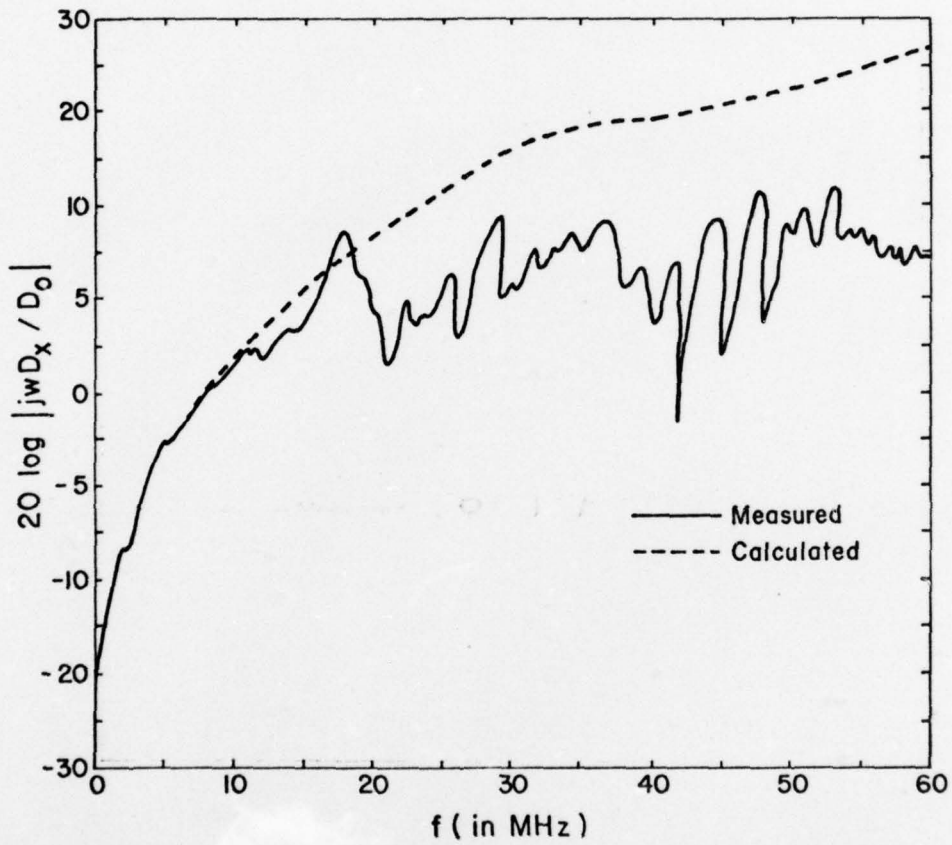


Figure 22: Evaluation of the CW performance of the ALECS facility -- electric field determination at the center of the working volume, $x = 0$, $z = 7.5$.

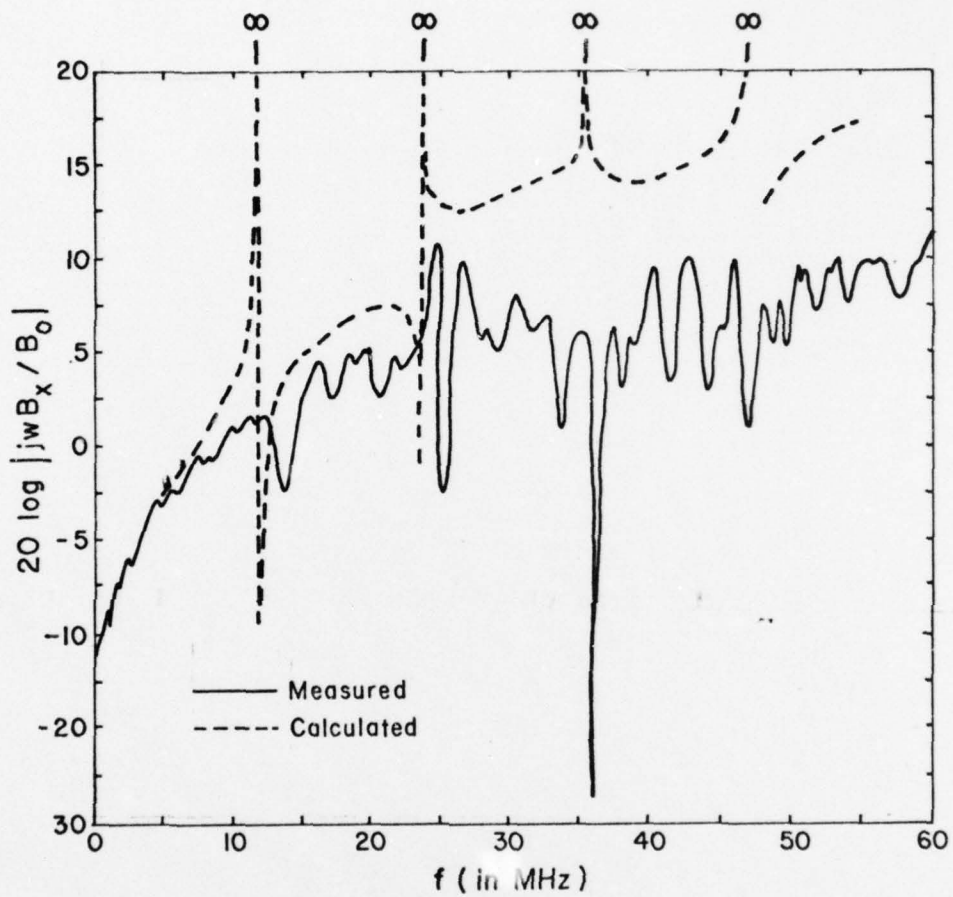


Figure 23: Evaluation of the CW performance of the ALECS facility-magnetic field determination at the center of the working volume, $x = 0$, $z = 7.5$.

However, for convenience in applying the inverse Fourier transform here the unit step with exponential damping is considered, i.e., $u(t)e^{-\alpha t}$ where $\alpha = 4.8 \times 10^5 \text{ s}^{-1}$.

The complex magnitude of the Fourier transform of the vertical electric field is shown in Figures 10 through 15. In contrast with the results of Figures 8 and 9 the Fourier transform of the vertical electric field does not exhibit singularities at the cavity resonances. Results appropriate for the ALECS and ARES simulators are given. Note that it is only when the frequency is above the lowest cut-off frequency that there is any z-dependence of the fields.

Time domain results for the vertical electric field are shown in Figures 16 through 21. These indicate that the TEM mode contribution is dominant.

f. Comparison of Experimental Data and Theoretical Results
for the ALECS Facility

In 1974 Giles et.al. [7] evaluated the performance of the ALECS facility in the CW mode. In particular, \dot{B} and \dot{D} measurements were made versus frequency at the center of the working volume. Figures 22 and 23 shown the results of these measurements. On the same figures one can see the results of the theoretical analysis for CW performance. In order to compare results, B_0 and D_0 were chosen such that the experimental and theoretical results matched at 5 MHz.

Before interpreting the foregoing results, the question of finite width versus infinite width plates should be considered. Marin [8] found that for finite width plates the TE modes were most important, i.e., they exhibited less attenuation above cutoff, and the analysis

used here did not include TE modes. However, to propagate TE modes the plates must support transverse currents and since the ALECS simulator (as well as the ARES simulator) is constructed with parallel wires rather than actual plates, the ALECS simulator will not propagate TE modes. And also since the TEM mode contributes very significantly to the simulator field there is good agreement between the measured and calculated data. The disparity increases significantly at higher frequencies primarily because the waveguide modes supported by the actual finite width waveguide are evanescent. The infinities in the calculated results occur since there are assumed to be no reflections in the conical input section.

3. Electromagnetic Fields in an Infinite, Parallel Plate Waveguide with a Double Conical Input Section

a. Physical Model

In some instances one wishes to obtain field values in the parallel plate region of a simulator that are higher than those attainable from a single pulser. In these situations, one solution is to use two separate pulsers and two input sections, Figure 24. One problem that arises is the nonsimultaneous firing of the sources, and the analysis must take this into account if it is to provide meaningful data.

b. Mathematical Model

As in section 2, each source is assumed to generate a spherical wave, \bar{E}

$$\bar{E} = v_o \frac{e^{-jkr}}{r} \hat{\theta} \quad (38)$$

where $r = (x \mp a/4) + (z + z_o)$ for the upper (-) and lower (+) cones. Again, normalizing each source to 1 volt, one obtains a magnetic source for the upper cone as

$$u_{M_y} = \frac{-z_o e^{-jk \left[\sqrt{(x - a/4)^2 + z_o^2} - \ell \right]}}{\theta_o [(x - a/4)^2 + z_o^2]} \quad (39)$$

For the lower cone, the magnetic source becomes

$$u_{M_y} = \frac{-z_o e^{-jk \left[\sqrt{(x + a/4)^2 + z_o^2} - \ell \right]}}{\theta_o [(x + a/4)^2 + z_o^2]} \quad (40)$$

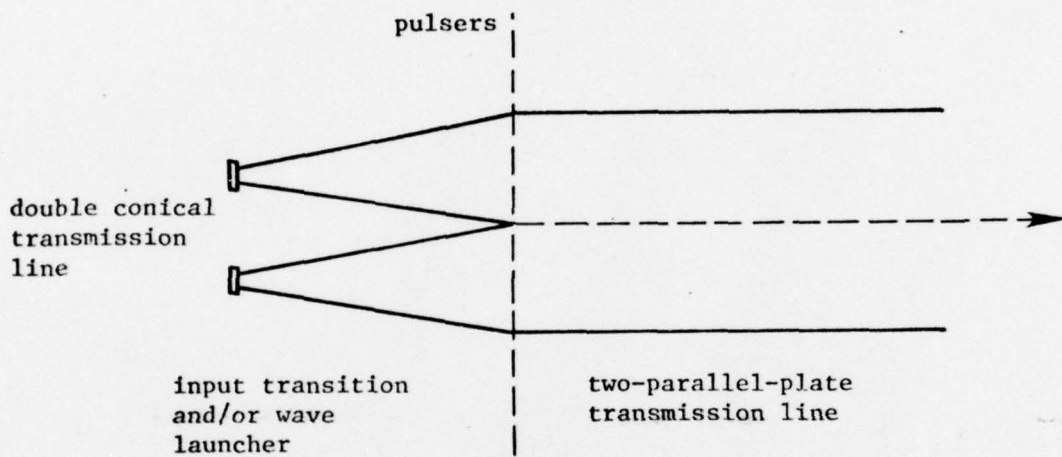


Figure 24: A Design for a Parallel-Plate Transmission Line Simulators. (View parallel to plates and perpendicular to direction of propagation, or z-direction.)

Substitution of (39) into (16) [the upper source analysis is performed independently of the lower source] leads to

$$u_{H_y^e}(x, z, \omega) = \frac{z_o \epsilon \omega}{\theta_o a} \sum_{n=0,2,4,\dots} \frac{\epsilon_n}{2} u_{A_n^e} \cos \frac{n\pi x}{a} \frac{e^{-jk_n z}}{k_n}, \quad z > 0 \quad (41)$$

where

$$u_{A_n^e} = \int_0^{a/2} \frac{\cos \frac{n\pi x'}{a}}{(x' - a/4)^2 + z_o^2} e^{-jk \sqrt{(x' - a/4)^2 + z_o^2}} dx' \quad (42)$$

and

$$u_{H_y^o}(x, z, \omega) = \frac{z_o \omega \epsilon e^{jkl}}{\theta_o a} \sum_{n=1,3,5,\dots} u_{A_n^o} \sin \frac{n\pi x}{a} \frac{e^{-jk_n z}}{k_n}, \quad z > 0 \quad (43)$$

where

$$u_{A_n^o} = \int_0^{a/2} \frac{\sin \frac{n\pi x'}{a}}{(x' - a/4)^2 + z_o^2} e^{-jk \sqrt{(x' - a/4)^2 + z_o^2}} dx' \quad (44)$$

For the lower cone one obtains expressions for H_y^e and H_y^o that are identical to (41) and (43) except $u_{A_n^e}$ and $u_{A_n^o}$ must be replaced by $l_{A_n^e}$ and $l_{A_n^o}$ where

$$l_{A_n^e} = \int_{-a/2}^0 \frac{\cos \frac{n\pi x'}{a}}{(x' + a/4)^2 + z_o^2} e^{-jk \sqrt{(x' + a/4)^2 + z_o^2}} dx' \quad (45)$$

and

$$l_{A_n^o} = \int_{-a/2}^0 \frac{\cos \frac{n\pi x'}{a}}{(x' + a/4)^2 + z_o^2} e^{-jk \sqrt{(x' + a/4)^2 + z_o^2}} dx' \quad (46)$$

For nonsimultaneous firing of the sources, (41) and (43) should be modified so that they differ in phase by $\omega\tau$ where τ is the time duration between the firings.

c. Time Domain, Magnetic Field

The step response for the even terms in the upper cone excitation is obtained as follows. Expression (41) is multiplied by the frequency spectrum of the step function

$$\pi \delta(\omega) + \frac{1}{j\omega}$$

and the Fourier transform is

$$u_{hy}^{se} = \frac{1}{2\pi} \int_{-\infty}^{\infty} \left[\pi \delta(\omega) + \frac{1}{j\omega} \right] \frac{z_o \epsilon}{a \theta_o} \sum_{n=0,2,4,\dots} \frac{\epsilon_n}{2} \cos \frac{n\pi x}{a} \cdot \int_0^{a/2} \frac{\cos \frac{n\pi x'}{a}}{(x' - a/4)^2 + z_o^2} e^{-j \frac{\omega}{c} \sqrt{(x - a/4)^2 + z_o^2}} dx' \cdot \omega e^{j \ell \frac{\omega}{c}} \frac{e^{-jz \sqrt{\frac{\omega^2}{c^2} - \left(\frac{n\pi}{a}\right)^2}}}{\sqrt{\frac{\omega^2}{c^2} - \left(\frac{n\pi}{a}\right)^2}} e^{j\omega t} d\omega \quad (47)$$

As in the single cone case in section 2, the ω integral can be performed analytically leading to

$$u_{hy}^{se}(x, z, t) = \frac{1}{a\eta} + \frac{z_o}{a\theta_o \eta} \sum_{n=2,4,\dots} \cos \frac{n\pi x}{a} \int_0^{a/2} \frac{\cos \frac{n\pi x'}{a}}{(x' - a/4)^2 + z_o^2} \cdot J_o \left\{ \frac{n\pi}{a} \left[\left[ct + \ell - \sqrt{(x' - a/4)^2 + z_o^2} \right]^2 - z^2 \right]^{1/2} \right\} dx' \quad (48)$$

with the restriction that $ct + l - \sqrt{(x' - a/4)^2 + z_0^2} \geq z$. In a similar fashion odd terms for the upper source, $u_{h_y}^{so}$, and even and odd terms for the lower source, $l_{h_y}^{se}$ and $l_{h_y}^{so}$ respectively, can be derived. Finally, if one allows the upper source to fire after the lower source by a time interval τ , one obtains

$$h_y^s(x, z, t) = u_{h_y}^{se}(x, z, t) + u_{h_y}^{so}(x, z, t) + l_{h_y}^{se}(x, z, \tau_1) + l_{h_y}^{so}(x, z, \tau_1) \quad (49)$$

where $\tau_1 = t + \tau$. In detail, (49) becomes

$$h_y^s(x, z, t) = \frac{2f_1}{a\eta} + \frac{z_0}{a\theta_0\eta} \sum_{n=2,4,6,\dots} \cos \frac{n\pi x}{a} \int_0^{x_u} \frac{\cos \frac{n\pi x'}{a}}{(x' - a/4)^2 + z_0^2} \left[J_0 \left\{ \frac{n\pi}{a} \sqrt{(ct + l - \sqrt{(x' - a/4)^2 + z_0^2})^2 - z^2} \right\} + J_0 \left\{ \frac{n\pi}{a} \sqrt{(c\tau_1 + l - \sqrt{(x' - a/4)^2 + z_0^2})^2 - z^2} \right\} \right] dx' + \frac{z_0}{a\theta_0\eta} \sum_{n=1,3,5} \sin \frac{n\pi x}{a} \int_0^{a/2} \frac{\sin \frac{n\pi x'}{a}}{(x' - a/4)^2 + z_0^2} \left[J_0 \left\{ \frac{n\pi}{a} \sqrt{(ct + l - \sqrt{(x' - a/4)^2 + z_0^2})^2 - z^2} \right\} - J_0 \left\{ \frac{n\pi}{a} \sqrt{(c\tau_1 + l - \sqrt{(x' - a/4)^2 + z_0^2})^2 - z^2} \right\} \right] dx' \quad (50)$$

The comments regarding the solution of (36) in section 2 are also applicable to the solution of (50).

d. Time Domain, Electric Field

Having derived $u_{H_y^S}(x,z,\omega)$ and $l_{H_y^S}(x,z,\omega)$, one can obtain the Fourier transform of the vertical electric field $E_x(x,z,\omega)$ from (24). Then, in exactly the same procedure as that described in section 2e, time domain electric fields may be obtained using the inverse Fourier transform. Also as before the electric field calculation is made for an exponentially-decaying, unit-step excitation.

e. Numerical Results for the ATLAS I Simulator

While the ALECS and the ARES simulators could not propagate TE modes, the ATLAS I simulator can since the waveguide plates are a wire mesh and hence can support currents transverse to the direction of propagation. Therefore, the results to be presented subsequently are valid only in a qualitative sense since the analysis did not include TE modes. However, the excitation of the TEM mode and the asynchronous firing of the pulses should be treated quite accurately by the analysis. Accordingly a copious amount of data is presented. Since the ATLAS I simulator is still under construction there is no measured data to validate the analysis. For a detailed discussion of the predicted behavior of the ATLAS I simulator the authors defer to references [9] through [12].

First the Fourier transform of the vertical electric field is shown for various positions within the ATLAS I simulator with an assumed typical asynchronous firing of the pulsers. Magnitude plots are given in Figures 25 through 28 for various points within the working volume.

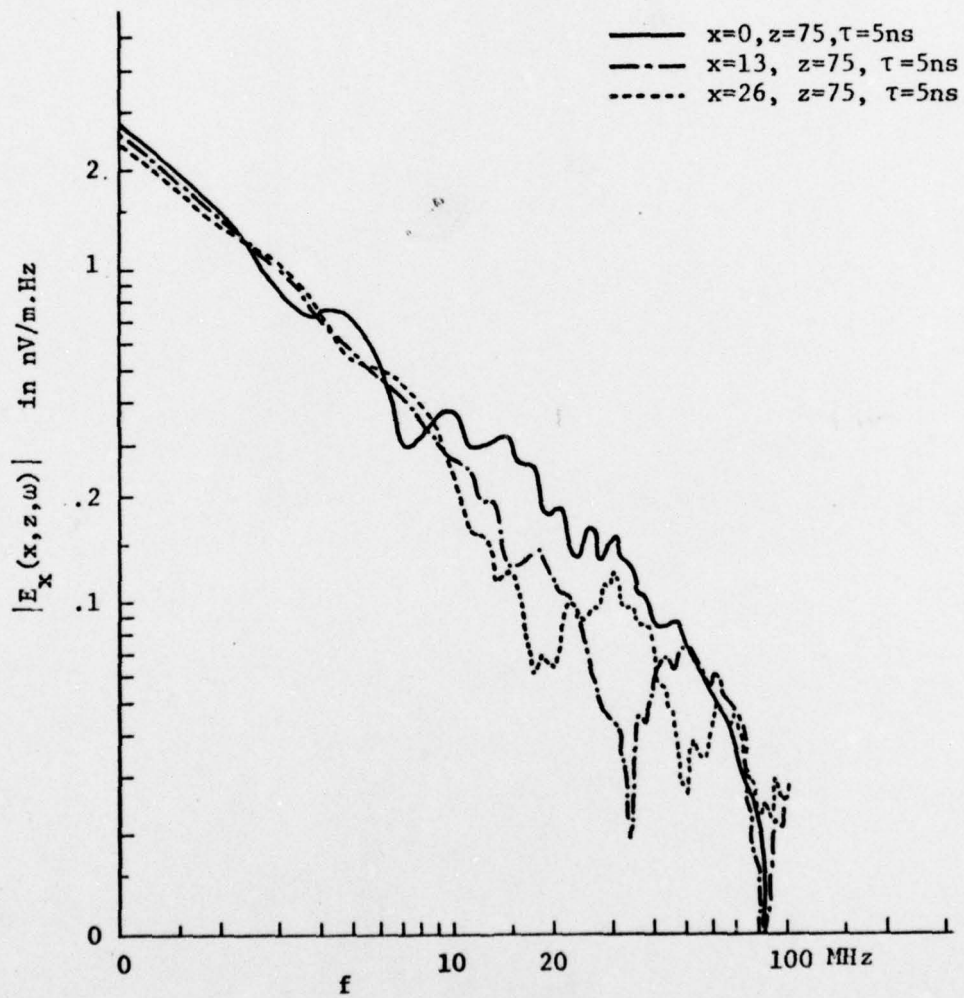


Figure 25: The Fourier transform of the vertical electric field produced by a unit step (with exponential decay) excitation of the ATLAS I simulator.

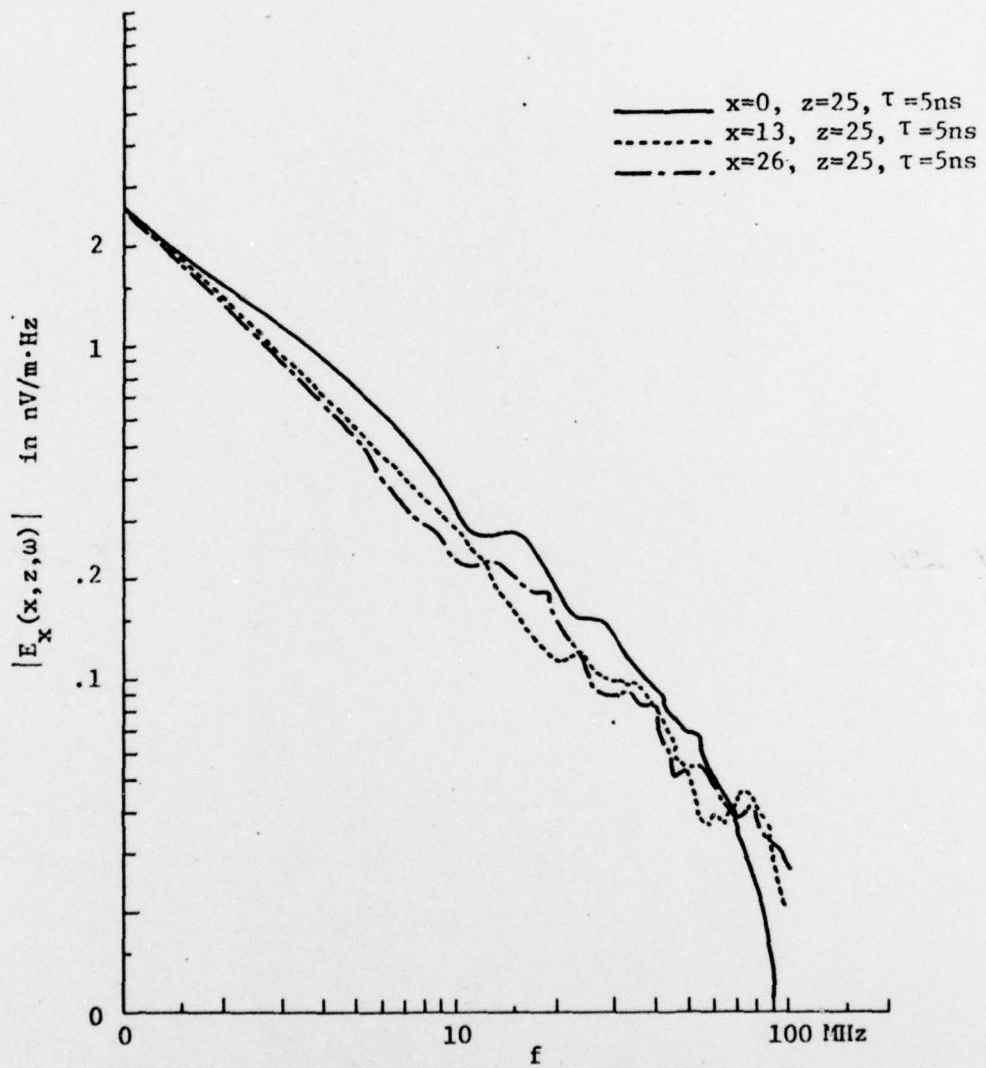


Figure 26: The Fourier transform of the vertical electric field produced by a unit step (with exponential decay) excitation of the ATLAS I simulator.

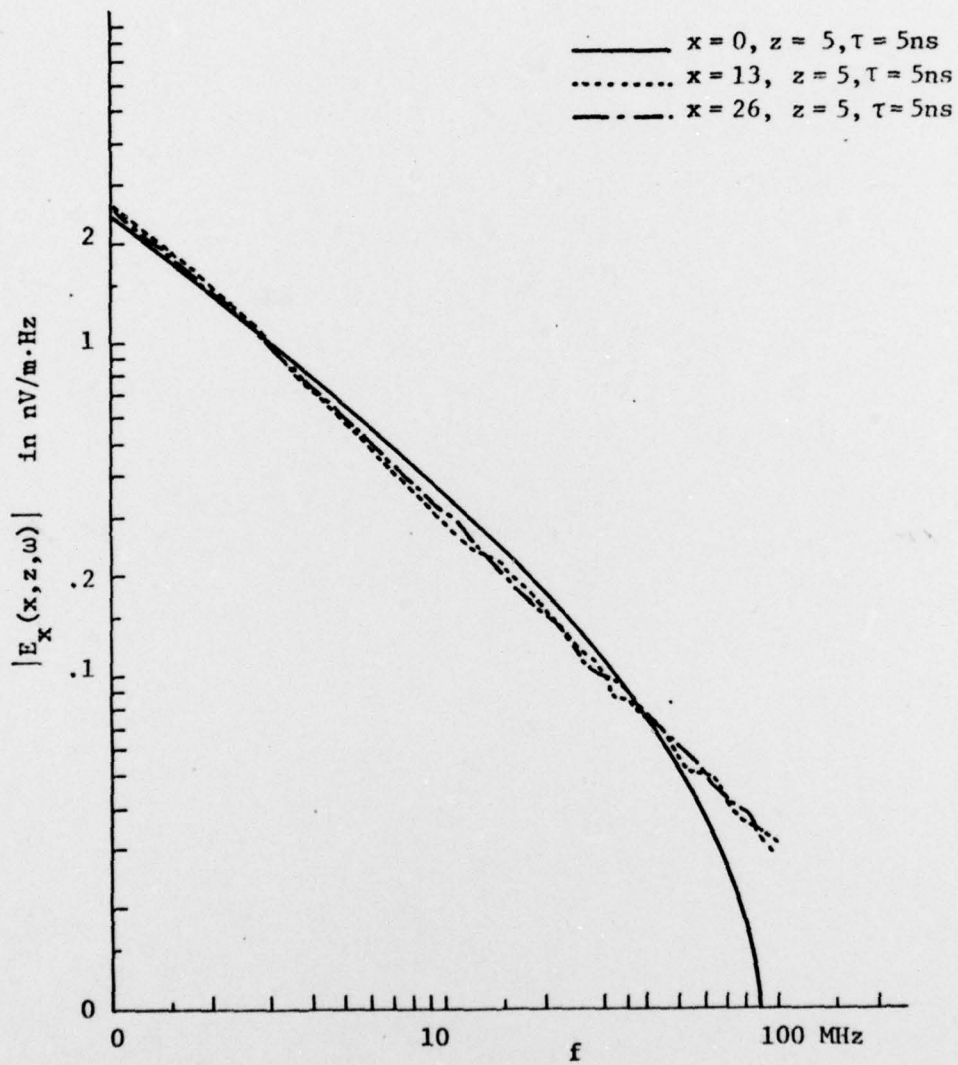


Figure 27: The Fourier transform of the vertical electric field produced by a unit step (with exponential decay) excitation of the ATLAS I simulator.

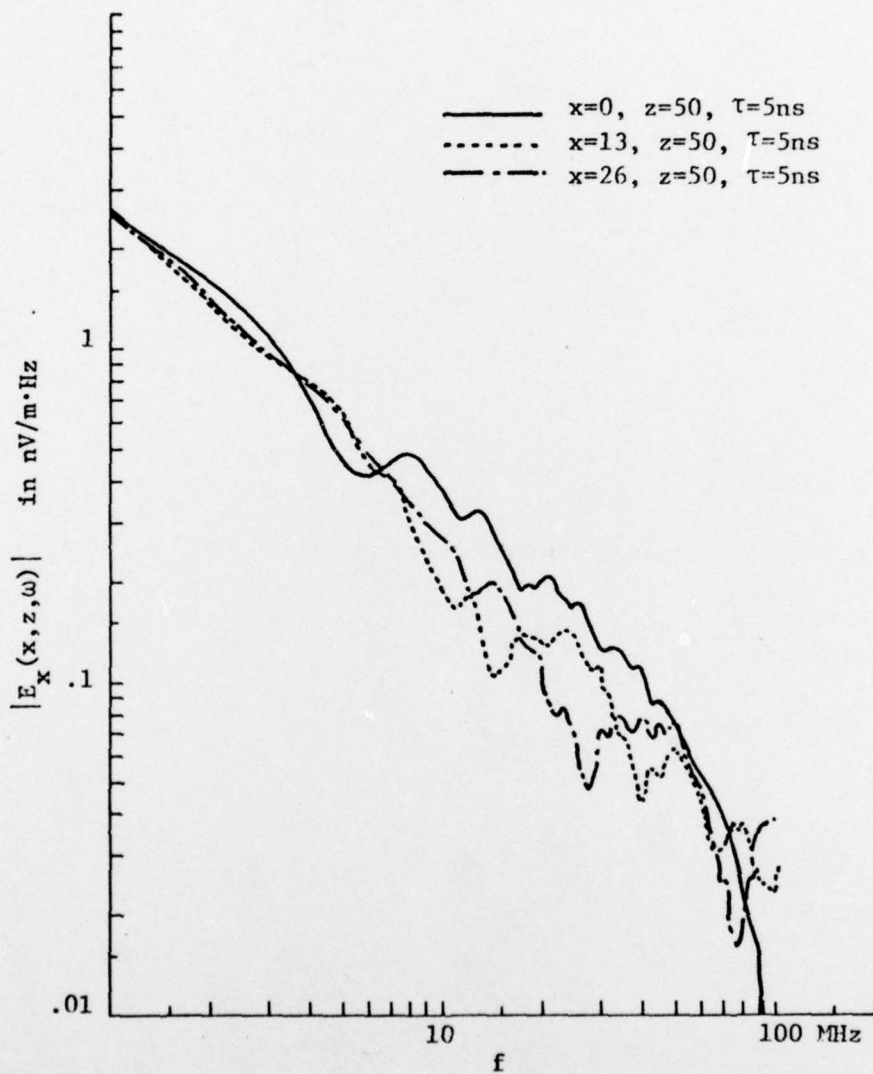


Figure 28: The Fourier transform of the vertical electric field produced by a unit step (with exponential decay) excitation of the ATLAS I simulator.

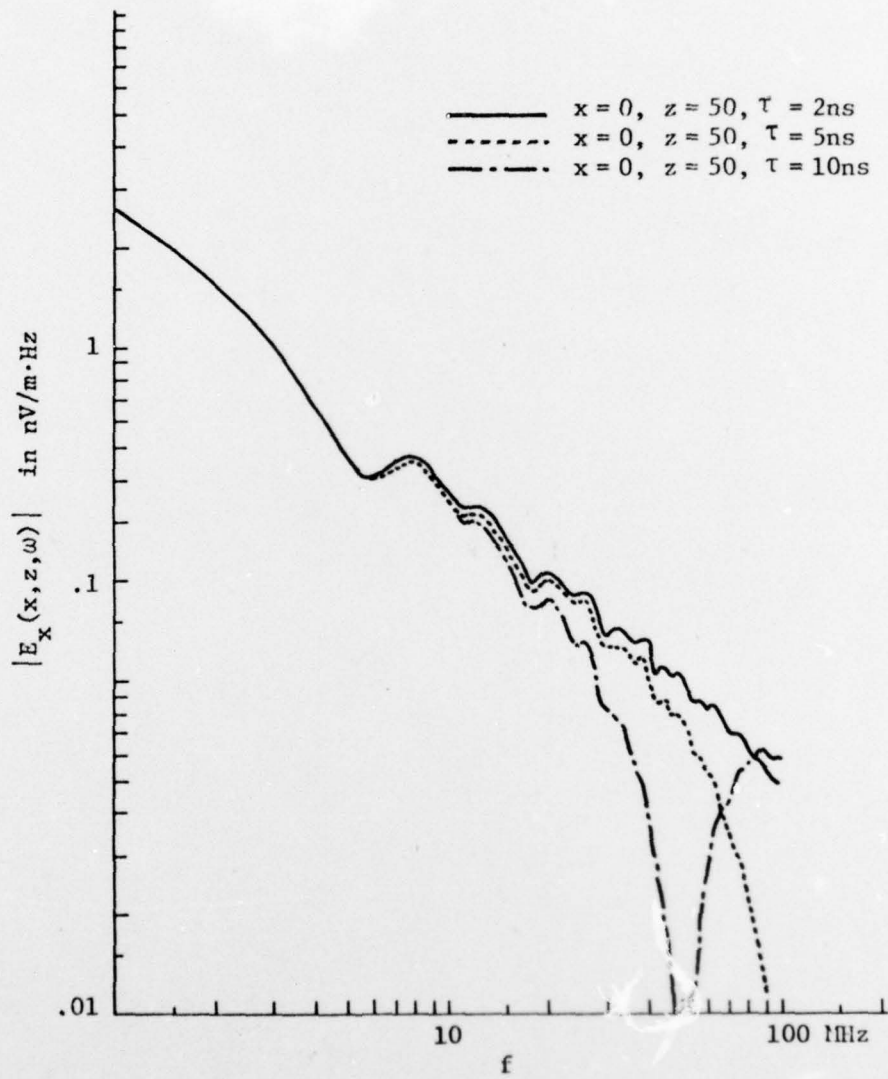


Figure 29: The Fourier transform of the vertical electric field produced by a unit step (with exponential decay) excitation of the ATLAS I simulator.

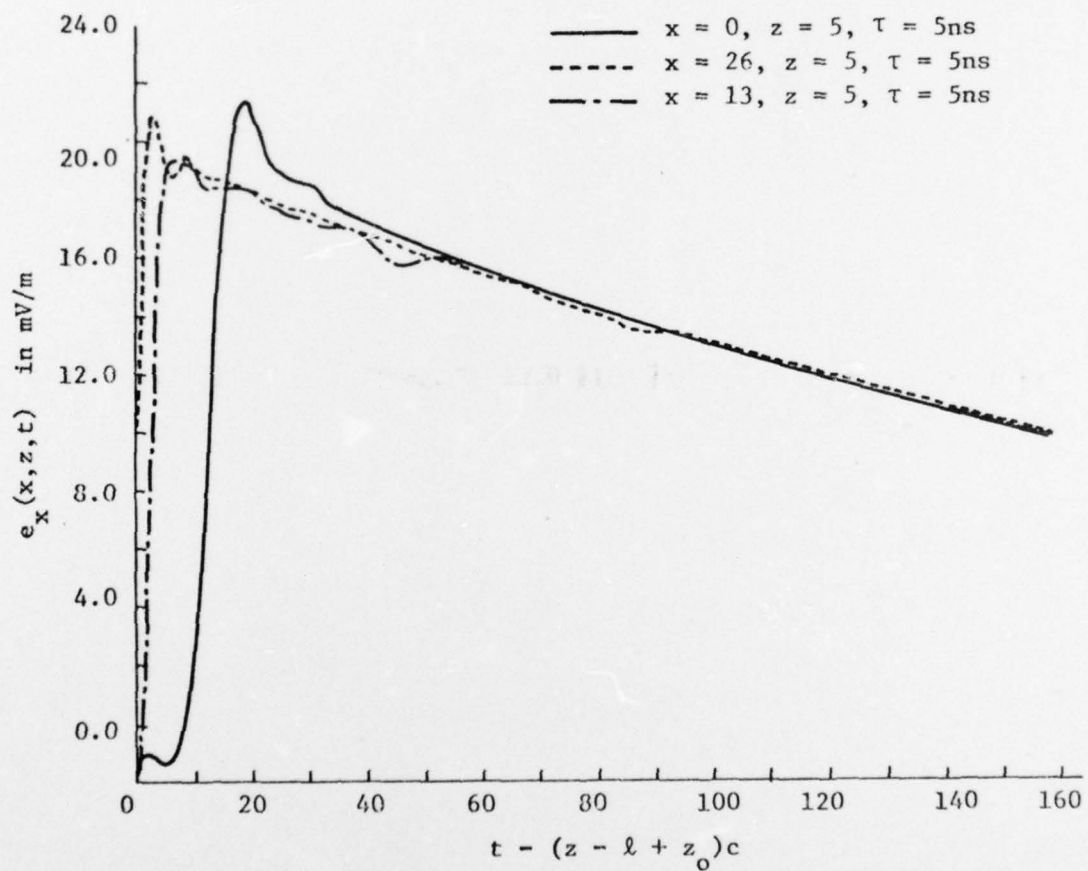


Figure 30: The vertical electric field produced by a unit step (with exponential decay) excitation of the ATLAS I simulator.

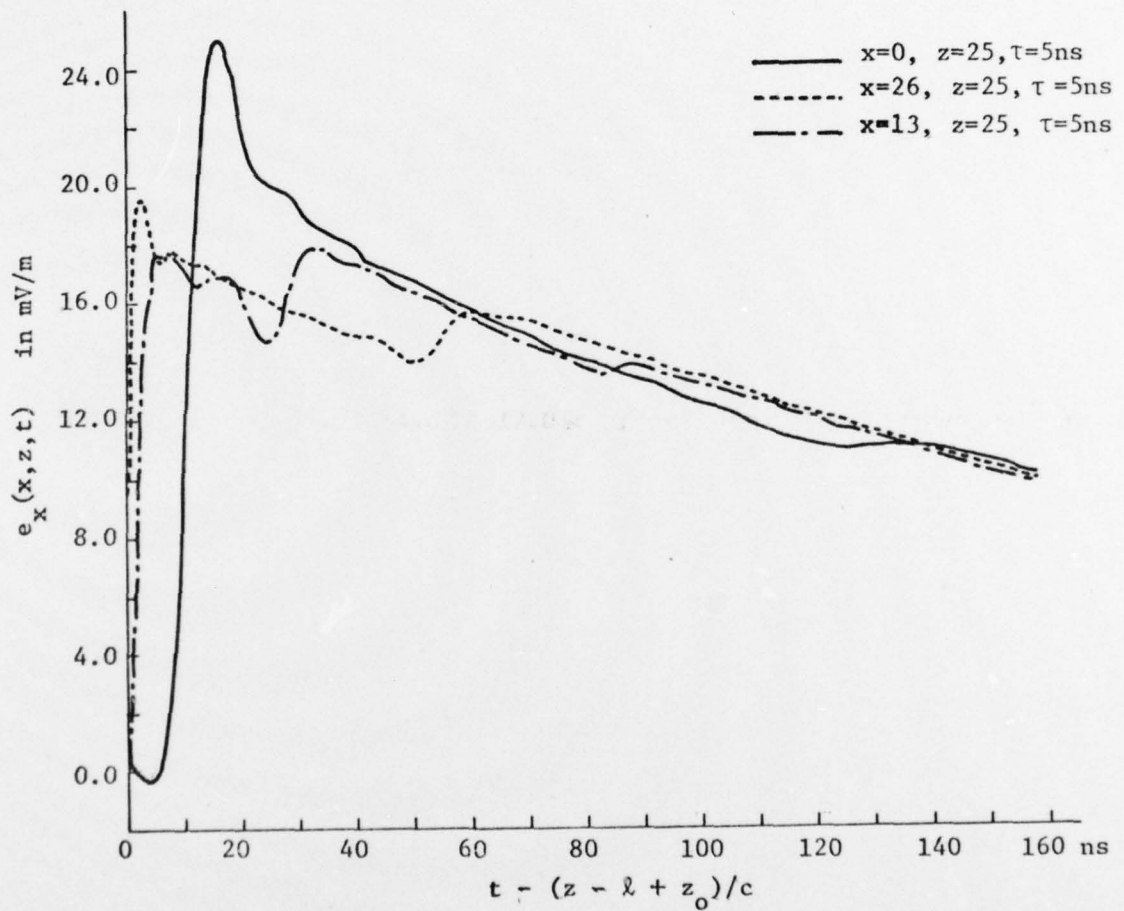


Figure 31: The vertical electric field produced by a unit step (with exponential decay) excitation of the ATLAS 1 simulator.

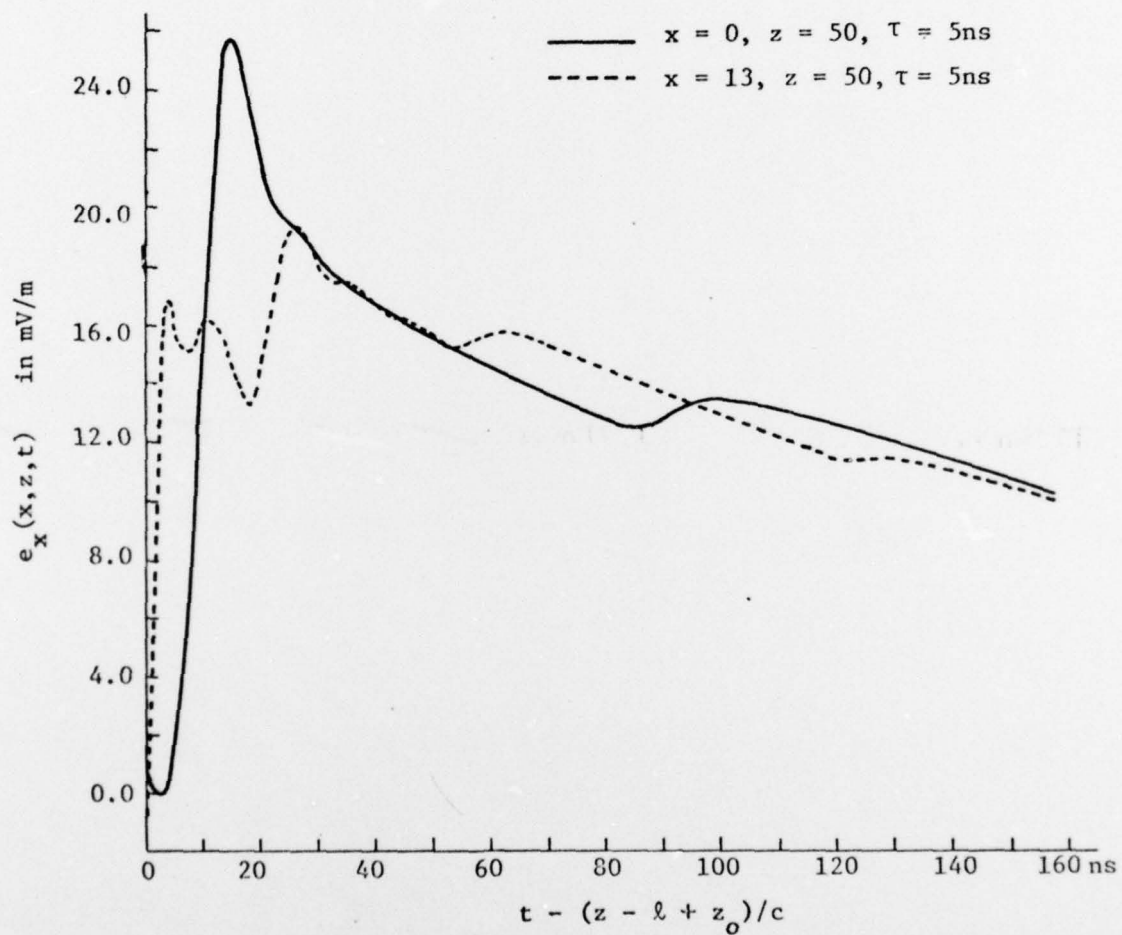


Figure 32: The vertical electric field produced by a unit step (with exponential decay) excitation of the ATLAS I simulator.

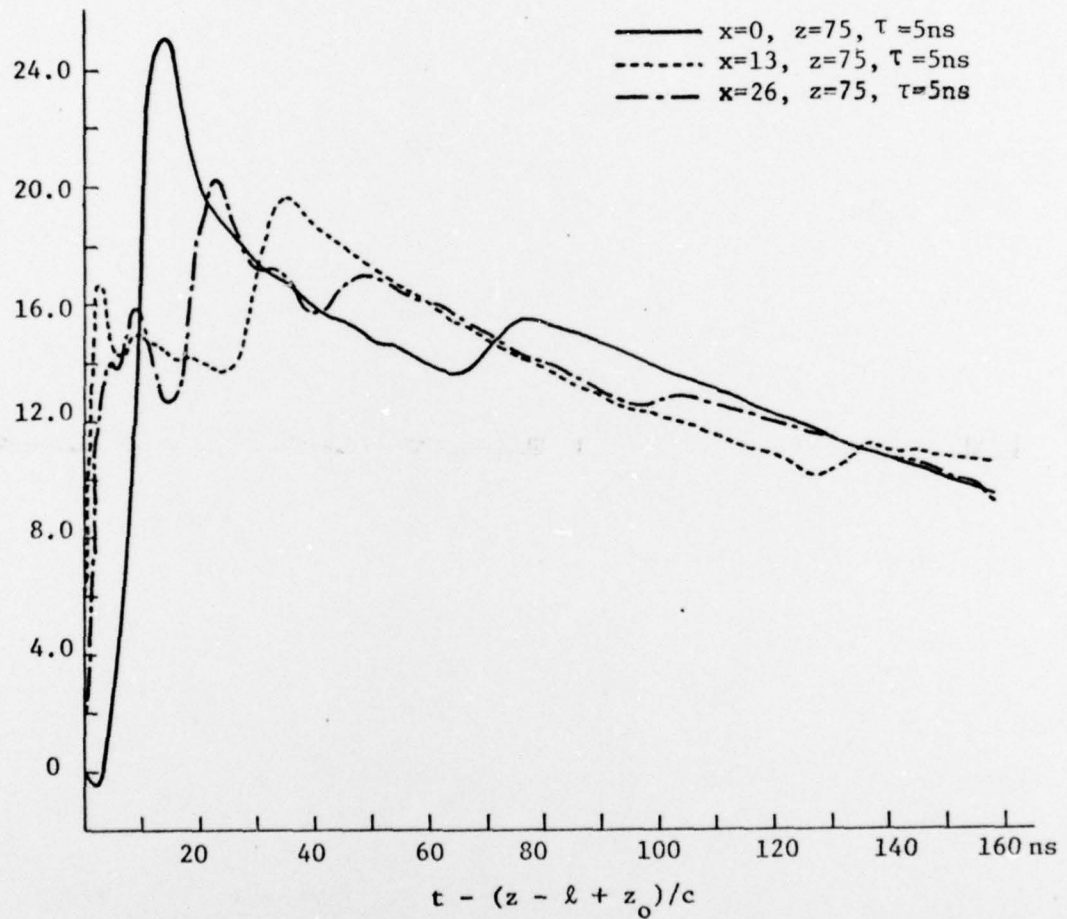


Figure 33: The vertical electric field produced by a unit step (with exponential decay) excitation of the ATLAS I simulator.

For a unit step excitation (even with exponential decay), the waveguide modes are much more significant for the ATLAS simulator than for the ALECS or ARES due to its dual input sections and due to its lowest cut-off frequency for the waveguide modes being only 5.7 MHz. It is readily noted that the higher order modes become increasingly significant with distance from the input transition section. If only a pure TEM mode were excited in the simulator then the magnitude plots of the Fourier transform would be straight lines.

A significant contribution to the excitation of the higher order modes is the asynchronous firing of the pulsers driving the input sections of the ATLAS simulator. This can be seen from figure 29. However, the deep nulls in the curves at 50 MHz and 100 MHz are due to destructive interference occurring as a result of the phase difference between the two sources of the two input sections

As mentioned in the foregoing the ATLAS I simulator can support TE modes whereas the analysis includes only TM modes. For finite width plates both the TE and TM modes are evanescent, but for infinite plates the modes do not radiate. Hence the effect of the TM modes is over emphasized by the analysis (as shown in Figures 22 and 23) and the effect of the TE modes under emphasized. One would expect then that the relative importance of the higher order modes as exhibited in Figures 25 through 28 should be representative. But the asynchronous effect as shown in Figure 29 should be quite accurate.

In Figures 30 through 33 the time domain vertical electric field is presented for an exponentially decaying unit step excitation of the dual input sections to the ATLAS I simulator. Note that at the center

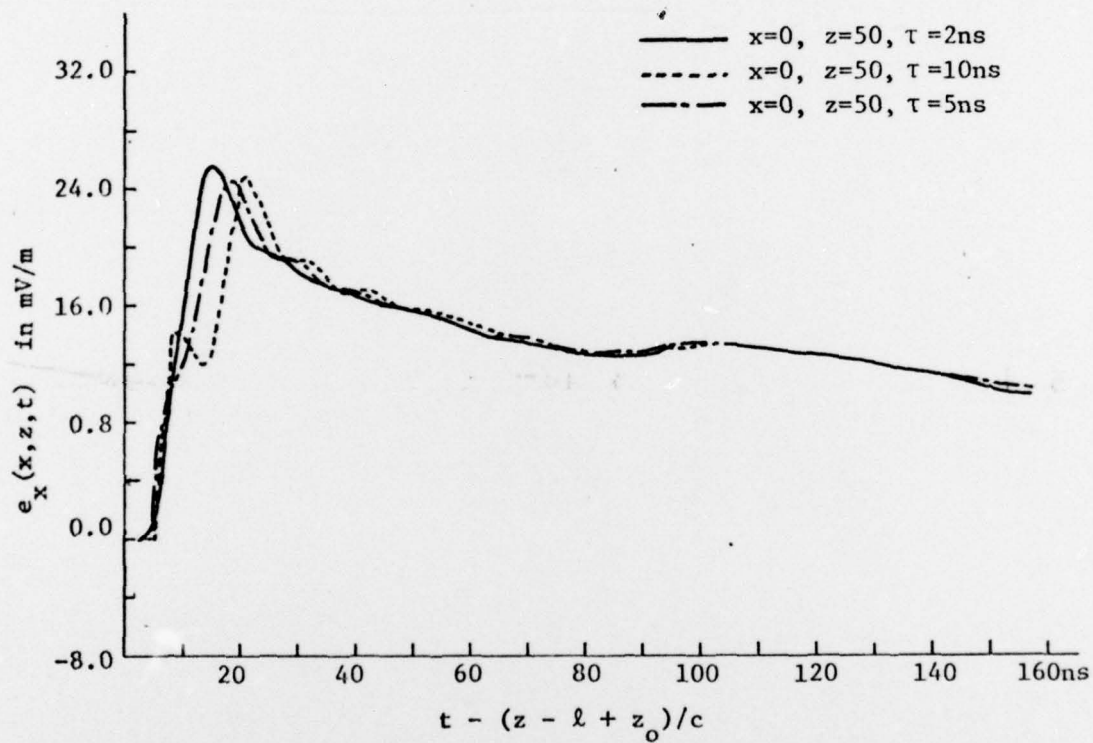


Figure 34: The vertical field produced by a unit step (with exponential decay) excitation of the ATLAS I simulator.

of the working volume ($x=0, z=50$) the peak electric field is about 26 millivolts/meter. Baum, et al. [12] predict that the value should be about 20 millivolts/meter. In arriving at their result Baum, et al. use ray theory primarily. It is further noted that the overall time domain response follows the prediction presented by Baum, et al, considering that their assumed excitation is a unit step. Also the general behavior at $x = 13, z = 50$ follows the roughly sketched waveform that Baum, et al. predict for their point c. They predict an initial peak of about 11 millivolts/meter whereas the present analysis yields about 17 millivolts/meter, which is quite satisfactory agreement in view of the completely different analyses that are used.

In their predictions of the electric field produced by the ATLAS I simulator Baum, et al. [12] do not consider asynchronous firing of the input pulsers. The effect in the electric field at the center of the working volume due to the nonsimultaneity of the excitations of the dual input sections is exhibited in Figure 34. First there is an increase in the rise time and second if the asynchronous time is sufficiently large, e.g. $\tau = 10$ ns , a precursor peak occurs. These precursor peaks are even more pronounced in the horizontal magnetic field computations as shown in Figure 35 for the same location in the simulator. The magnitude of the Fourier transform of the horizontal magnetic field is shown in Figure 36 for a typical location in the ATLAS I simulator.

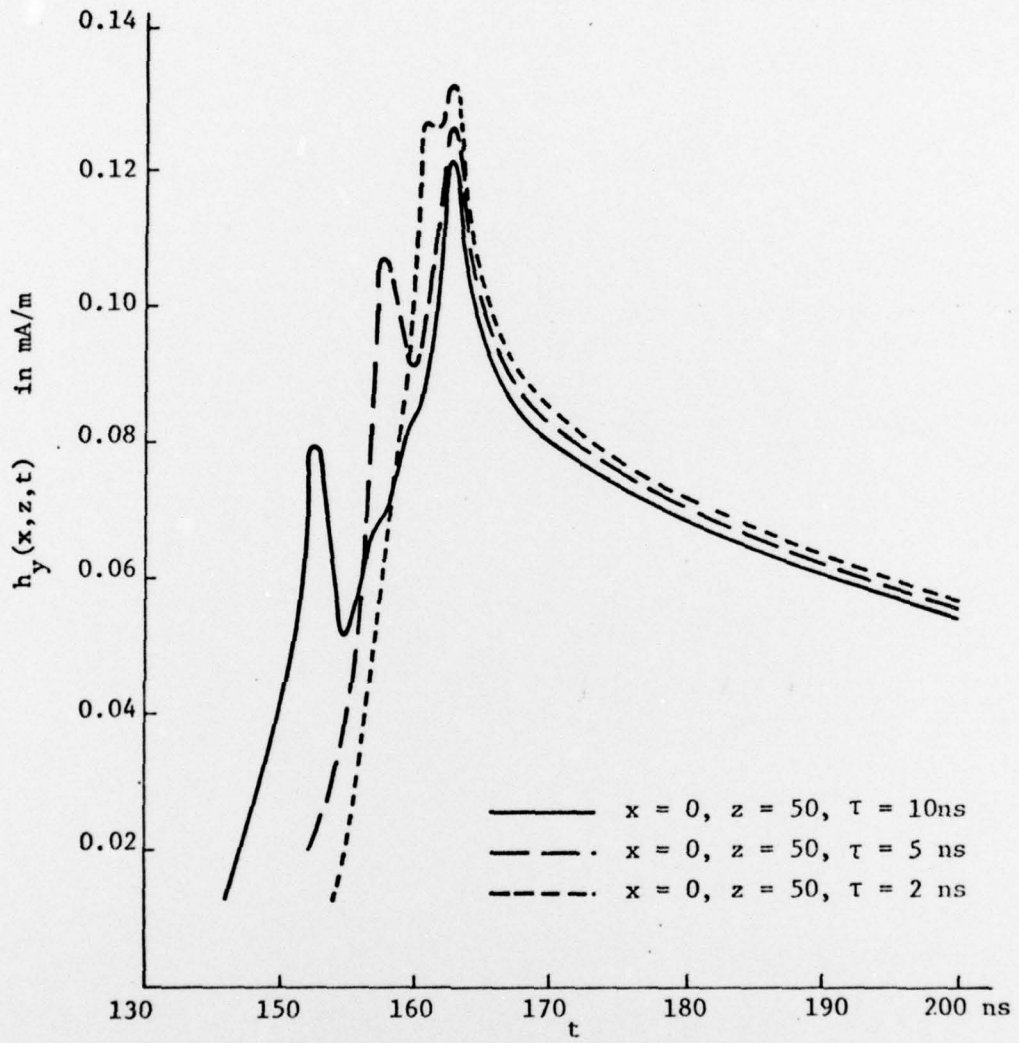


Figure 35: The horizontal magnetic field produced by a unit step excitation of the ATLAS I simulator.

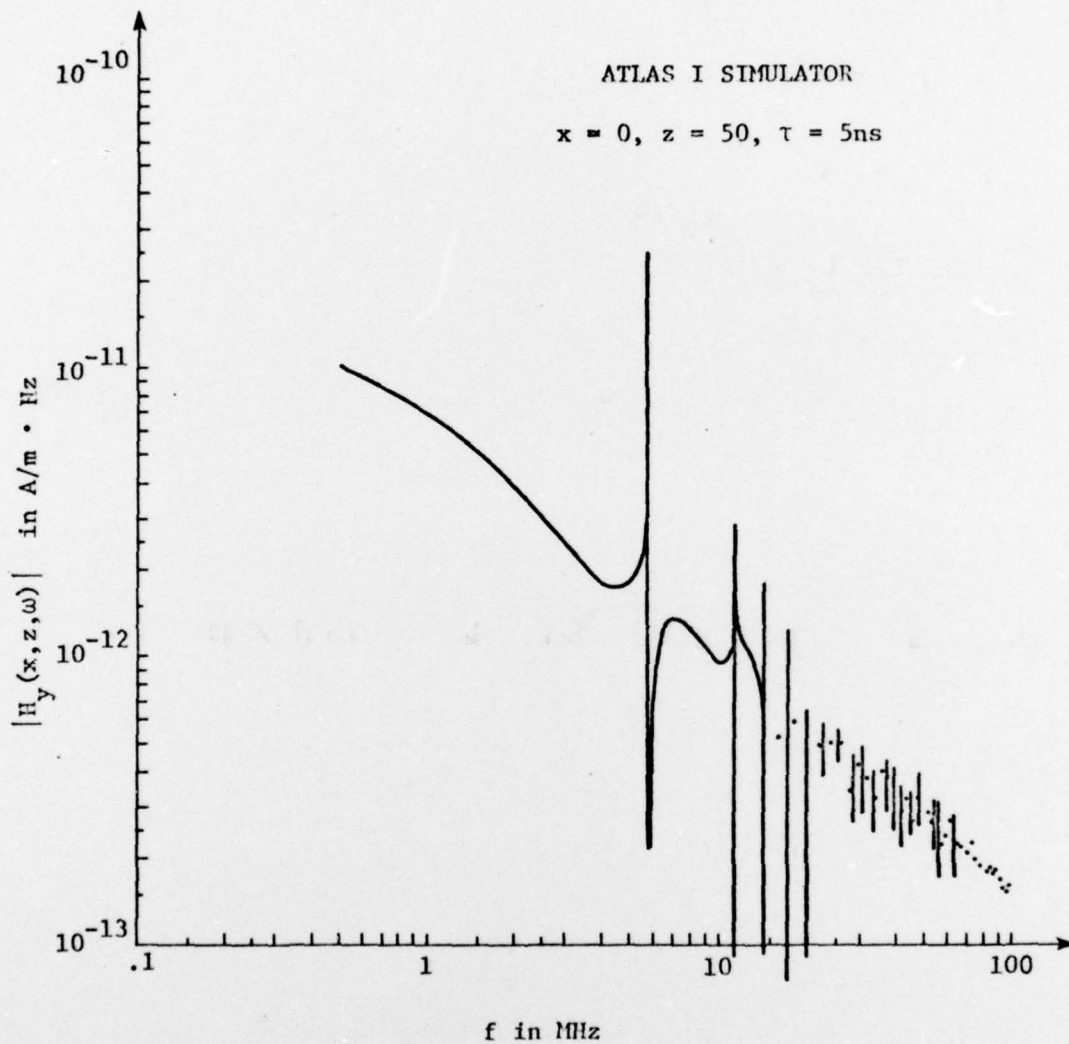


Figure 36: The Fourier transform of the horizontal magnetic field produced by a unit step excitation of the ATLAS I simulator.

References

1. Baum, C. E., "Impedances and Field Distributions for Parallel Plate Transmission Line Simulators," Sensor and Simulation Note 21, Air Force Weapons Laboratory, Kirtland AFB, N.M., Jan., 1966.
2. Brown, T. L. and K. D. Granzow, "A Parameter Study of Two Parallel Plate Transmission Line Simulators of EMP," Sensor and Simulation Note 52, Air Force Weapons Laboratory, Kirtland AFB, N.M., Apr. 1968.
3. Marin, L., "Modes on a Finite-Width, Parallel-Plate Simulator I Narrow Plates," Sensor and Simulation Note 201, Air Force Weapons Laboratory, Kirtland AFB, N.M., Sept. 1964.
4. Dudley, D. G. and J. P. Quintenz, "Multi-Modal Transient Excitation Effects in an Infinite, Parallel-Plate Wave Guide," Can. Jour. of Physics, 50, 2826 (1972).
5. Taylor, C. D. and T. T. Crow, "Induced Electric Currents on Some Configurations of Wires, Park I, Perpendicular Crossed Wires," Interaction Note 85, Kirtland AFB, N.M., Nov. 1971.
6. Campbell, G. A. and R. M. Foster, Fourier Integrals for Practical Applications. D. Van Nostrand Co., New York, p. 11. 1948.
7. Giles, J. C., M. K. Bumgardner, G. Seely, and J. Furaus, "Evaluation and Improvement of the CW Performance of the ALECS Facility," EG & G Report AL-1085, 29 July 1974.
8. Marin, L., "Modes on a Finite-Width, Parallel-Plate Simulator II. Wide Plates," Sensor and Simulation Note 223, Air Force Weapons Laboratory, Kirtland AFB, N.M., March 1977 (revised September 1977).
9. Higgins, D., "The Diffraction of an Electromagnetic Plane Wave by Interior and Exterior Bends in a Perfectly Conducting Sheet," Sensor and Simulation Note 128, Air Force Weapons Laboratory, Kirtland AFB, N.M., January 1971.
10. Baum, C. E., "General Principles for the Design of ATLAS I and II, Part I: ATLAS: Electromagnetic Design Considerations for Horizontal Version," Sensor and Simulation Note 143, Air Force Weapons Laboratory, Kirtland AFB, N.M., January 1972.
11. Baum, C. E., et al., "Electromagnetic Design Calculations for ATLAS I, Design 1," Sensor and Simulation Note 153, Air Force Weapons Laboratory, Kirtland AFB, N.M., June 1972.
12. Baum, C. E., D. F. Higgins, and D. V. Giri, "Pulser Test Results and Preliminary Estimation of Transient Electric Field Waveforms in ATLAS I," ATLAS Memo 18, Kirtland AFB, N.M., October 1976.



**DEPARTMENT
OF
ELECTRICAL ENGINEERING**



**ENGINEERING AND
INDUSTRIAL RESEARCH STATION**

**MISSISSIPPI STATE UNIVERSITY
STATE COLLEGE, MISSISSIPPI**